Self-Assembled Monolayers As Models For Silica

Francisco T. Cavadas

Thesis submitted to the Faculty of Virginia

Polytechnic Institute and State University in partial

fulfillment of the requirements for the degree of

Master of Science

In

Chemistry

Paul A. Deck, Chairman

Mark R. Anderson

Brian E. Hanson

August 15, 2001

Blacksburg, Virginia

ABSTRACT

The reaction of hydroquinone and 1,12-dibromododecane affords 4-(12-bromo-dodecyloxy)phenol (**4**, 7% yield). The alkyl bromide (**4**) was converted to the corresponding thiol with thiourea to afford 4-(12-mercaptododecyloxy)phenol (**1**) in 52% yield. The reaction of t-butyllithium with 4-bromoanisole followed by reaction with 1-12-dibromododecane affords a mixture of 4-bromoanisole, 1,12-dibromododecane ,and 4-(12-bromododecyl)-anisole (**6**). Silica gel chromatography resulted in an inseperable mixture of 4-bromoanisole and (**6**). Reaction of the mixture with BBr_3 afforded 4-(12-bromododecyl)phenol (**7**) in 34% yield. The alkyl bromide (**7**) was converted to the corresponding thiol with thiourea to afford 4-(12-mercaptododecyl)phenol (**2**) in 9% yield. Reduction of 16-mercaptohexadecanoic acid with BH_3•THF afforded 16-mercaptohexadecanol (**3**) in 53% yield. All new compounds were characterized by ^{1}H NMR, ^{13}C NMR, transmission IR, HRMS, and, where possible, elemental microanalysis.

Self-assembled monolayers (SAMs) on gold were prepared using thiols **1**, **2**, and **3**. SAMs were characterized using reflectance-absorbance infrared spectroscopy (RAIRS). Diagnostic vibrational modes were assigned by comparing RAIRS spectra to normal mode frequencies and intensities calculated using DFT methods at the 6-31G* level using commercial software. Water droplet goiniometry found contact angles of 52^{o}, 53^{o}, and 64^{o} for SAMs prepared from **1**, **2**, and **3**, respectively. SAMs of **1** and **2** were found to be hydrophilic. When SAMs prepared from **1**, **2**, and **3** were silylated with phenyldimethylchlorosilane, the resulting contact angles were 78^{o}, 74^{o}, and 75^{o} respectively. A significant increase in contact angles for silylated SAMs of **1** and **2** indicated facile silanization of the surface hydroxides. RAIRS spectra were also obtained for the functionalized SAMs. Silylated SAMs prepared from **1**, **2**, and **3** are currently under investigation as models for silica-immobilized metallocene olefin polymerization catalysts.

ACKNOWLEDGMENTS

First of all I would like to thank my parents and my brother for all their love, encouragement, and support. They have allowed me to pursue my interests and have always provided for my every need.

I would also like to thank my undergraduate professors in chemistry which encouraged me to pursue a degree in chemistry and who patiently took the time to explain concepts to me when I had trouble with the subject matter. I would specially like to thank Dr. Leo A. Bares who has been my mentor for so many years and to whom I owe so much.

I would also like to thank Dr. Mark Anderson, and Dr. Brian Hanson for their guidance and instruction.

I would also like to thank the members of my research group: Matt Thornberry, Eric Hawrelak, Owen Lofthus, and Xu Cheng for your helpful discussions, assistance in lab and for putting up with me all this time.

Last but not least I would like to thank my wife Maria Elena Gulias Placias for all her support and patience. Thank you for putting up with my frustrations for the last two years. I love you more than words can say. Esta tesina te la dedico a ti. Te amo muchisimo.

Table of Contents

List of Figures

List of Schemes

List of Tables

Chapter 1

1.1 Statement of objectives

The goal of this research was to prepare a series of -OH terminated self-assembled monolayers (SAMs) for use as models for silica. These hydroxyl-terminated SAM surfaces represent "well-defined" models of the surface of hydroxylated silica. By studying the behavior of –OH terminated SAMs toward silylation, the immobilization of $BrSiMe_2$-functionalized zirconocene dibromides on partially dehydroxylated silica was modeled. The characterization of compounds **1**, **2**, and **3** (Figure 1) was carried out using various techniques, particularly surface reflectance infrared spectroscopy (RAIRS). RAIRS can provide a series a of spectroscopic "fingerprints" for SAMs of **1**, **2**, and **3** and was used to establish the spatial orientation of the surface –OH groups. Because the ultimate goal of this work is to understand catalyst immobilization on silica, Sections 1.1-1.6 of this introductory chapter will present some background on prior synthesis and characterization of immobilized metallocene olefin polymerization catalysts. Because this work also involves SAMs on gold substrates, some background is provided in Sections 1.7- 1.11 of this introduction and will illustrate some of the key concepts and methods used in SAM chemistry. Chapter 2 describes our design for a "silica model" SAM and the synthesis and characterization of three specific hydroxy-terminated thiols (**1**, **2**, and **3**) (Figure 1) adsorbed on gold substrates that serve as a preliminary implementation of this design.

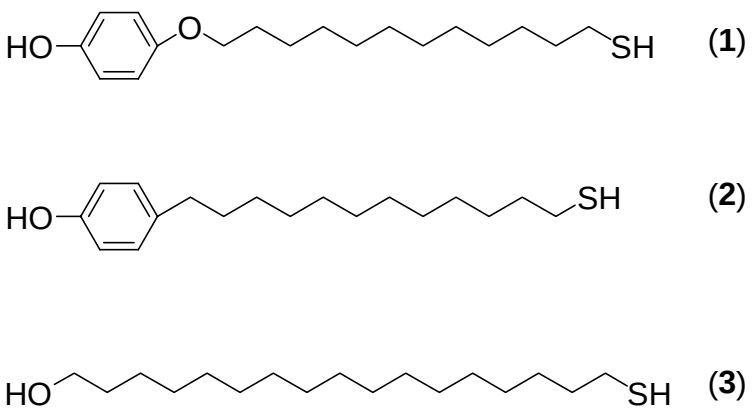

Figure 1 Compounds 1**,** 2**, and** 3 **used in SAM preparation**

Chapter 3 describes the characterization of these SAMs by RAIRS, the use of computational methods to assign and interpret the RAIRS spectra, and the effects of silylating agents on the RAIRS spectra and water droplet surface contact angles of the three model monolayers.

1.2 Metallocene Immobilization for Olefin Polymerization

Increasing demand for polyolefins has prompted the plastics industry to develop new polymers with properties different from those produced by conventional Ziegler-Natta (ZN) catalysts. Improving the manufacturing efficiency and physical properties of existing polyolefins remains an important goal too. The industrial response to this twofold demand has been to develop new catalysts and processes that can produce a broader range of resins in the context of existing high-volume process technologies.

Group 4 metallocenes are an attractive family of olefin polymerization catalysts for several reasons. They are single-site catalysts, at least in solution, which means activity, molecular weight, tacticity, branch content, and chain structure are uniform from chain to chain. Their mechanism of action is well characterized. The relationship between metallocene structure and polymer properties are highly developed.[1]

One of the major current industrial challenges problems is to adapt metallocenes to large-scale *heterogeneous* processes. Most importantly, the catalyst must be immobilized on a finely divided inert support in order to be used in a gas phase reactor. The next few sections summarize recent research in the heterogenization of metallocene catalysts. For comparison, some of the problems associated with "second generation" Ziegler-Natta catalysts are discussed. Industrial applications of heterogenized metallocenes to olefin polymerization are also presented. The review concludes with a discussion of various characterization methods that are employed in an effort to elucidate structure-property relationships of immobilized metallocenes and ongoing efforts by the author and others to contribute to this area.

1.2.1 Ziegler-Natta Catalysts

Ziegler and Natta independently discovered that mixtures of $TiCl_4$ and aluminum alkyls catalyze rapid ethylene and propylene polymerization. Previously, ethylene and propylene had been polymerized by free-radical initiated reactions that afford only highly branched, amorphous polyethylene. In contrast, Ziegler-Natta polyethylene and polypropylene is typically linear and highly crystalline. Ziegler's and Natta's research efforts clearly prompted much of the growth in polyolefin chemistry in the last 40 years.[1] The plastics industry still relies heavily on these "traditional" Ziegler-Natta catalyst systems as well as free radical processes to produce most polyolefins. However, it is important to understand some of the limitations of Ziegler-Natta catalysts.

1.2.2 First Generation Ziegler-Natta Catalysts

Ziegler-Natta (ZN) catalysts are combinations of transition metal halides, alkoxides, or alkyls with aluminum alkyls.[2] The active catalytic species are quasi-soluble and can polymerize ethylene at low pressures and at temperatures of 20-50 ^{o}C up to 120 ^{o}C. Millions of tons of polyethylene and polypropylene are produced per year with these catalysts.[2] Figure 2 illustrates some types of polymers that can be synthesized with first generation ZN catalysts, in addition to various polyethylene grades.

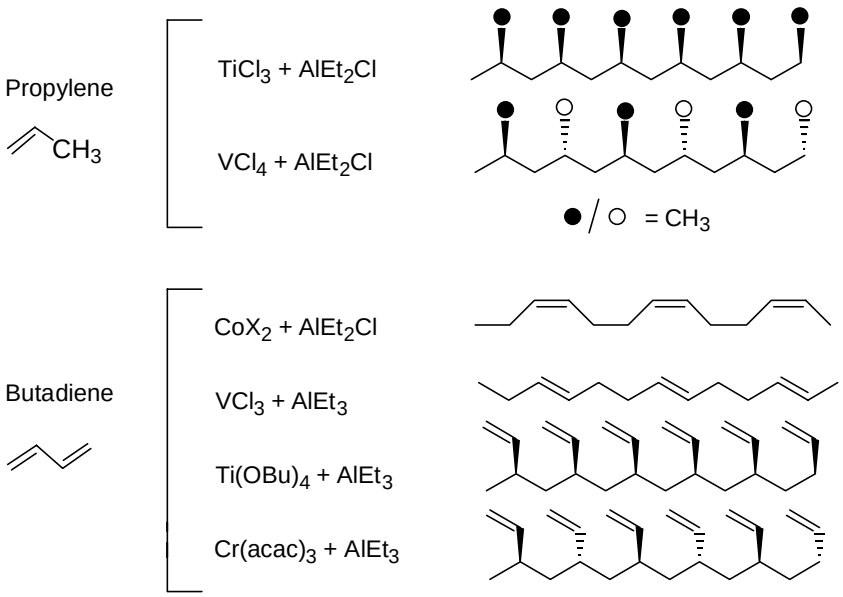

Figure 2 Polymers synthesized using Ziegler-Natta catalysts[3]

Despite these successes, problems remained in industrial applications and in the fundamental scientific understanding of the mechanism of the catalytic process. The catalytic species needed to be deactivated after polymerization, the solvent removed in order to purify the polymer, and the amount of residual catalyst (ash), which is incorporated into the polymer,

minimized. Extracting catalyst residue is costly and wasteful. These additional steps diminish the advantages of homogeneous ZN catalysts.[2]

1.2.3 Second Generation Ziegler-Natta Catalysts

Second generation catalysts are supported first generation catalysts and are strictly heterogeneous. Polymerization can be carried out in a solvent medium (slurry) or in the gas phase (fluidized bed). Immobilization on a support also disperses the catalyst and provides more exposed catalytic sites, increasing the activity per mole of transition metal. Bimetallic interactions between catalyst metal atoms can impede catalytic activity, but by immobilizing the catalyst, such bimolecular deactivation is minimized. Also, catalyst particle size can be better controlled with supports like $MgCl_2$ or silica allowing for uniform distribution of catalytic species throughout the polymerization medium. Unlike first generation catalysts, the molecular weight distribution of the polymer is narrow.[2] Gas phase ethylene polymerizations are also effected by supported chromium catalysts.[2] Solvents are not necessary in gas phase polymerizations, so polymer processing is greatly simplified.[2]

One fundamental problem with second generation ZN catalysts is that they are inherently multi-site catalysts. Active transition metal species occupy positions on the particle surface but not all active centers have the same ligand environments, because they reside in different crystal faces of the support or even in defect sites.[1] Although better than first-generation catalysts, second-generation ZN catalysts give polymers with higher molecular weight distributions (MWD) than single-site soluble catalysts. Yet, polymers with high polydispersities are useful and have some advantages – they are more processable because of their wider melting and softening ranges.

1.2.4 Recent Trends in ZN Catalyst Development

Ongoing research efforts focus on further improving the selectivity of the Ziegler-Natta system by using alternative support surfaces, activators, or support procedures but since the ZN catalyst field is mature, most advances are incremental. Progress in ZN catalysis is limited mainly to fine details or refinements rather than completely new ways of doing ZN catalysis. The search for "additives" and new support/activator combinations[4] is endless. Most research is driven by what is patentable rather than by what is useful.

Due to the increasing interest in broadening the range of linear low-density polyethylene grades available, much of the recent work is focussed on copolymerization. Many researchers have tried to develop statistical models for monomer insertion, but the work is complicated by various "synergistic" interactions between different monomers in copolymerizations.[5] From an experimental standpoint, copolymerization kinetics is tricky because ethylene and propylene are supercritical under ordinary polymerization conditions, therefore simple relations like Henry's Law aren't useful. Mechanistic studies such as these add to what is known about ZN catalysis but also emphasize the difficulties associated with thoroughly understanding all aspects of the catalysis.

1.2.5 Inorganic Support Surfaces for Second Generation Catalysts

Magnesium chloride was historically the surface of choice for immobilizing Ziegler-Natta catalysts.[6,7] Isotope labeling studies show that 24% of titanium centers attached to $MgCl_2$ in Ziegler-Natta catalysts are isospecific whereas 76% are aspecific.[8] One approach to achieving an isospecific catalyst is to modify the support in some way to improve the fraction of isospecific sites. Another is to selectively poison the aspecific sites with a Lewis base like methyl benzoate.

Exxon researchers found that adding a halogenating agent after treatment of silica with dialkylmagnesium further controls surface hydroxyl group reactivity.[9,10]

Recently, silica has superseded $MgCl_2$ as the preferred immobilization surface for Ziegler-Natta catalysts. Direct interaction of $TiCl_4$ with SiO_2 does not produce a suitably active catalyst.[11] However, dehydroxylation of silica followed by reaction with alkylaluminum compounds or alkylaluminum halides and $TiCl_4$ yields a highly active catalyst for ethylene polymerization and copolymerizations with 1-alkenes.[12,13] Magnesium alkyls are also used for decreasing surface reactivity and controlling the number of reactive surface hydroxyl groups.[14] Several patents issued to Mobil describe combinations of silica and organomagnesium compounds to provide a bifunctional support surface[9,15,16] which is then reacted with $TiCl_4$ to give a catalyst used for the synthesis of linear low density polyethylene (LLDPE) used for blown films. These patents claim that an initial hydroxyl group content of silica of 0.3 to 0.7 mmol/g is preferred for catalyst impregnation.

Partially hydroxylated magnesium oxide and titanium tetrachloride, following activation by triethylaluminum also gives a catalyst that produces $2x10^5$ g of polyethylene per gram of titanium,[17,18] although the importance of these other oxides is small relative to SiO_2. There are several important advantages of silica as a catalyst support. First, the particle size in both slurry and gas-phase polymerization processes is controllable.[6] Silica avoids the problem of chloride residue, which can change the polymer color when $MgCl_2$ is used. Halogens are also corrosive toward reactor equipment. Also, lower Al/transition metal ratios are needed to obtain high catalyst activities, which is important because alkyl aluminum compounds are expensive and lead to higher ash content. In addition, silica supported ZN catalysts are less expensive, which also significantly lowers polymer manufacturing costs.[6]

1.2.6 Catalyst Immobilization Methods

The primary support method for Ziegler-Natta catalysts involves a direct reaction of the support surface with $TiCl_4$. Under N_2, a slurry of the solid support and a solvent is stirred. Liquid $TiCl_4$ is added dropwise while stirring. Subsequently the mixture is heated. The solvent is volatized, and the remaining solid is dried under N_2.[19] The catalyst is then activated with aluminum alkyls, typically triethylaluminum.[20,21] In some cases magnesium alkyls are used.[13]

In cases where silica is used as the support, dehydroxylation is performed to remove excess surface hydroxyl groups.[6] Excess loading of catalyst does not increase polymerization activity. This means overloading simply wastes transition metal, and it can also increase binuclear degradation processes. Surface passivation with $EtAlCl_2$ also controls the number of surface hydroxyl groups while providing superior anchoring sites for the catalyst metal centers.[13] By reacting surface OH groups with alkylaluminum halides, a covalently bonded -O-AlX_2 surface species is obtained, which cannot migrate and prevents undesirable reactions of remaining OH groups with other components of the catalyst.[13]

Scheme 1 illustrates what is thought to occur when silica is passivated with $EtAlCl_2$ and reacted with $TiCl_4$ followed by activation with RMgCl.

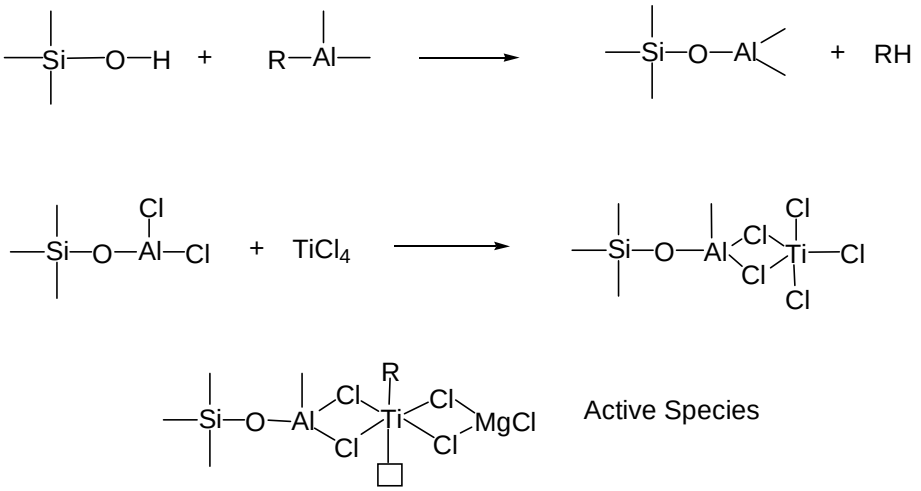

Scheme 1

Research into the preparation of different Ziegler-Natta systems involves varying support surfaces, passivating agents, and catalyst activators. This approach has resulted in a tremendous number of heterogeneous catalysts that form the backbone of the polyethylene and polypropylene industries[6] A recent review by Pullukat and Hoff[6] details some of the past and current patent literature on silica-supported Ziegler-Natta catalysts.

1.3 Metallocenes

After Wilkinson[22] and others developed synthetic approaches to group 4 metallocenes in the mid 1950s, the possibility of using complexes like Cp_2TiCl_2 as soluble, well-defined, single-site versions of Ziegler-Natta catalysts (e.g. $TiCl_4$) was obvious to scientists in academia and industry alike. Unfortunately, several problems were encountered immediately. For example, although mixtures of Cp_2TiCl_2 and $AlClEt_2$ polymerized ethylene at moderate reaction rates (Cp = C_5H_5), propylene was not polymerized at all.[23,24] Also, titanocene catalysts were not directly applicable in industrial processes due to their propensity to reduce to inactive Ti(III) species, limiting catalyst lifetimes. However, they served as useful homogeneous models for the individual steps of the catalytic mechanism due to their solubility in hydrocarbons.[11] Subsequently, Sinn[25] and Kaminsky[26] discovered that partially hydrolyzed aluminum alkyls, in

particular methylalumoxane (MAO), tremendously increase polymerization activities of metallocenes, and interest in metallocenes reawakened.[11] Importantly, they showed that Cp_2ZrCl_2/MAO catalyzes propylene polymerization with high activity. Figure 3 illustrates the activation of zirconocene dichloride by MAO.

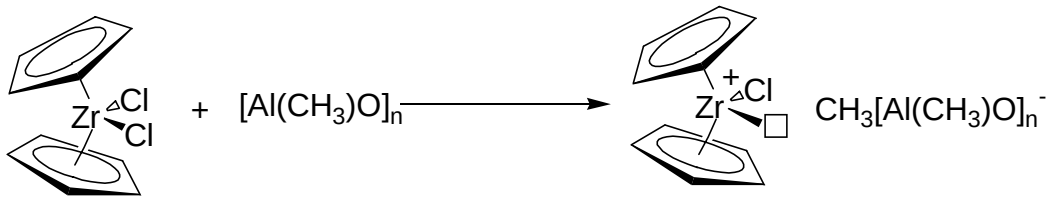

Figure 3 Activation of zirconocene dichloride with MAO

Substitution of the cyclopentadienyl (Cp) ancillary ligand influences solubility, activity, polymer molecular weight, and other microstructural aspects,[27] such as comonomer incorporation.[28] Replacement of the Cp ligands by substituted tetrahydroindenyl or fluorenyl ligands[29] also leads to catalysts that polymerize propylene with high stereospecificity.[29]

1.4 Immobilized Single-site Catalysts

Commercial polymerization processes that use homogeneous catalysts are suitable only for low crystallinity polymers, which remain soluble in the reaction solvent. In these cases the solvent is volatized and the polymer subsequently processed.[11] As with Ziegler-Natta catalysts, the need to support metallocenes to make polymerizations more economical has prompted significant academic and industrial research to immobilize metallocenes and develop single-site catalysts for gas-phase polymerizations.

In slurry processes the polymer has both high density and high crystallinity and therefore insoluble in most solvents. Ideally, these resins are produced in the gas phase. For this to work, however, the catalyst also must not significantly desorb from its support surface in order to avoid reactor fouling due to polymer adhering to reactor walls or stirring devices.[11] Figures 4 and 5[30]

illustrate the differences between a conventional slurry polymerization process and a gas phase reactor.

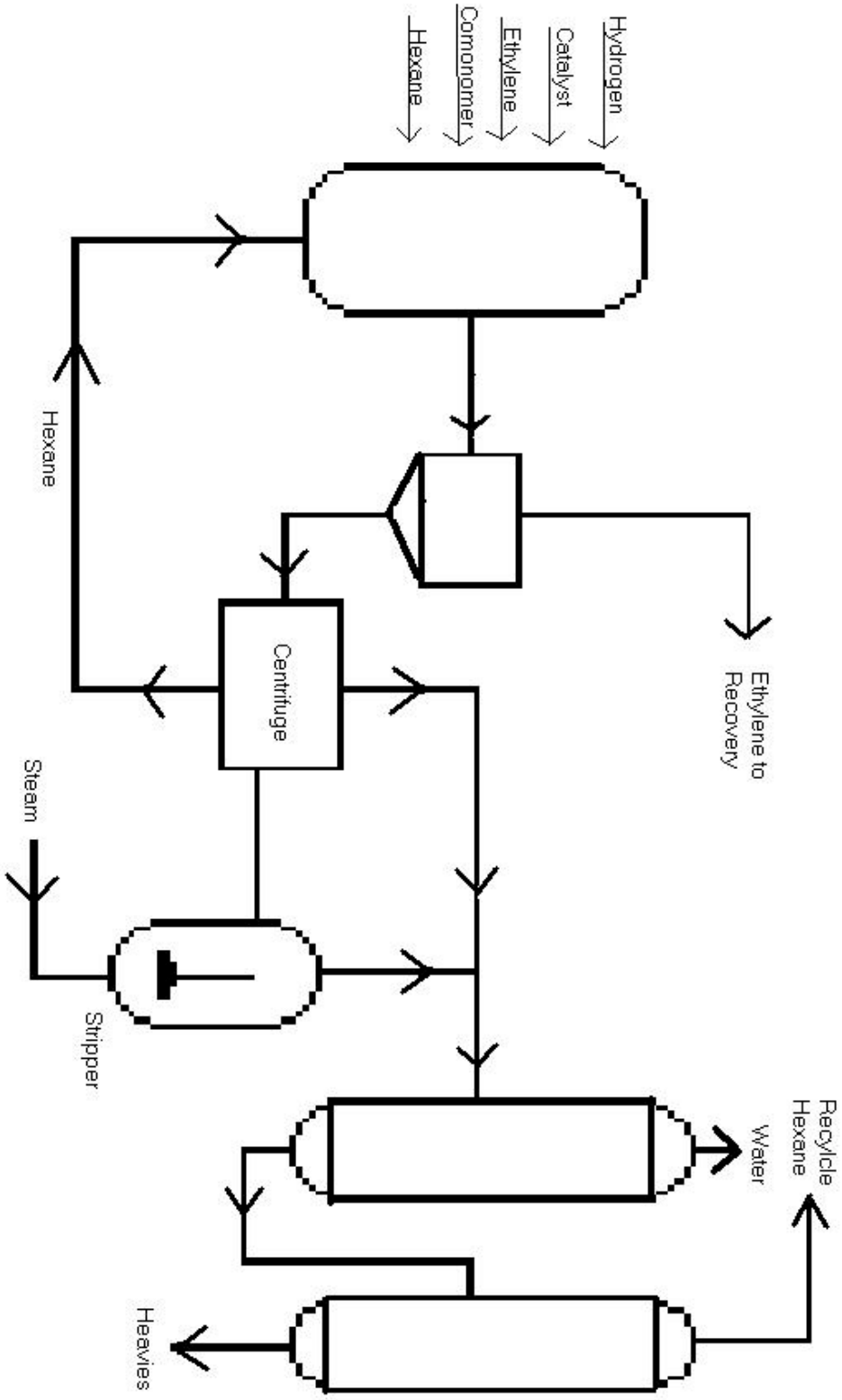

Figure 4 General reactor design for stirred slurry polymerization

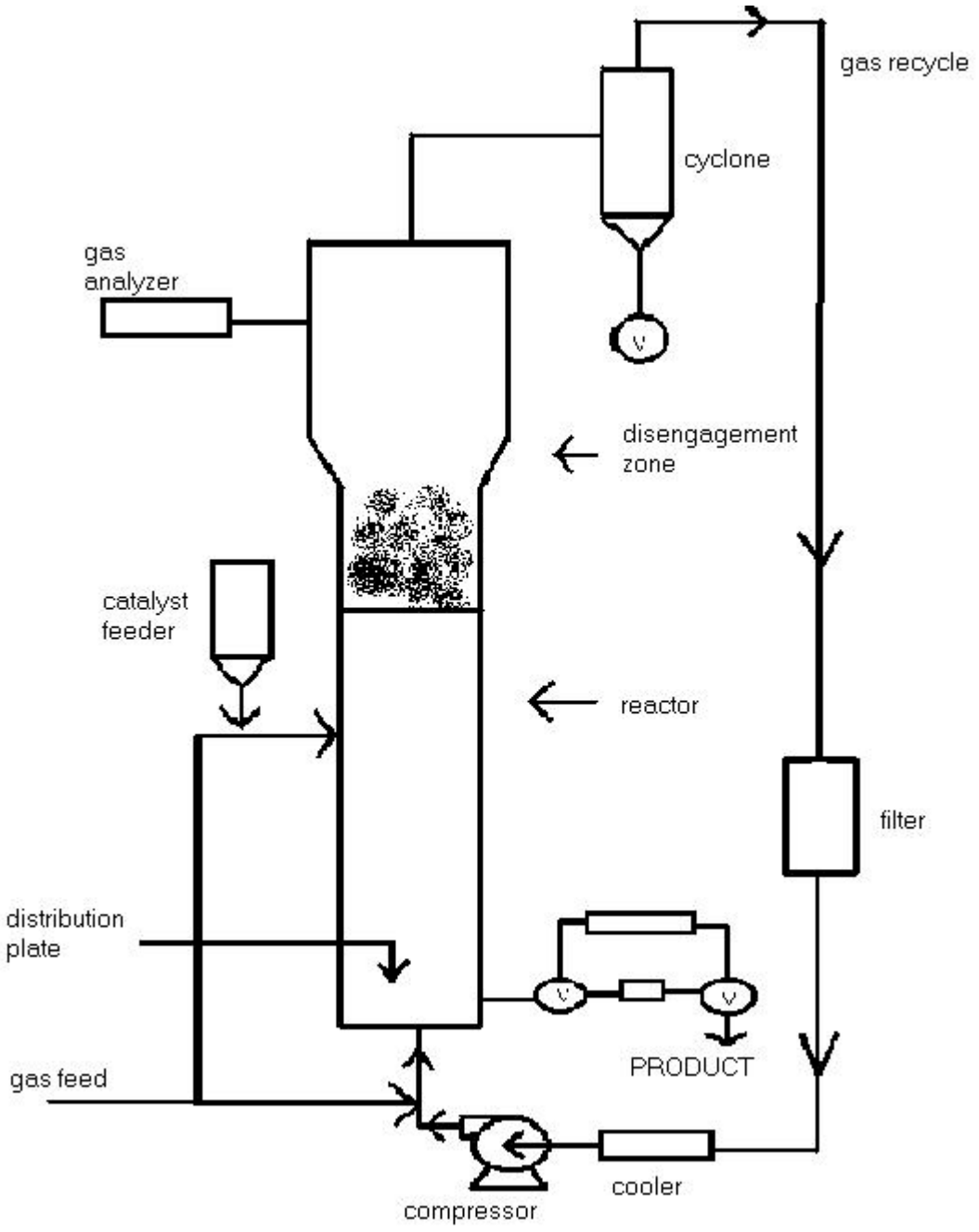

Figure 5 General reactor design for gas-phase polymerization

Thus, the requirements of commercial gas-phase reactors and the tailorability of metallocene structure led naturally to the development of "immobilized" single site catalysts. Single site catalysts have been successfully anchored onto various supports and are currently used in industrial plants to produce polymers of high molecular weight, high bulk density, and narrow molecular weight distributions.[11] This section describes the most important substrates and the methods of attaching metallocenes to them.

1.4.1 Inorganic Support Surfaces for Single-site Catalysts

The vast majority of single-site catalysts are activated by MAO and are supported on inorganic oxides.[11] Magnesium chloride is not used as extensively with single-site catalysts as it is with Ziegler-Natta catalysts, although patents using $MgCl_2$ have been issued as recently as 1992.[31] Bailly et al. reacted Cp_2ZrCl_2 with $MgCl_2$ in toluene and activated with MAO to produce spheroidal catalyst particles suitable for producing polyethylene or an ethylene copolymer.[31] Soga and coworkers supported $(Cl_2Si(Ind)_2)ZrCl_2$ on $MgCl_2$. Activation by MAO results in a catalyst which polymerizes propylene isotactically.[32] The catalyst (Figure 6) can either bind to $MgCl_2$ via the chlorines on the siloxy bridge (A) or through the chlorines on the Zr (B). Polymerization studies suggest that Catalyst A is the most active form, although it is 100 times less active than its homogeneous counterpart.

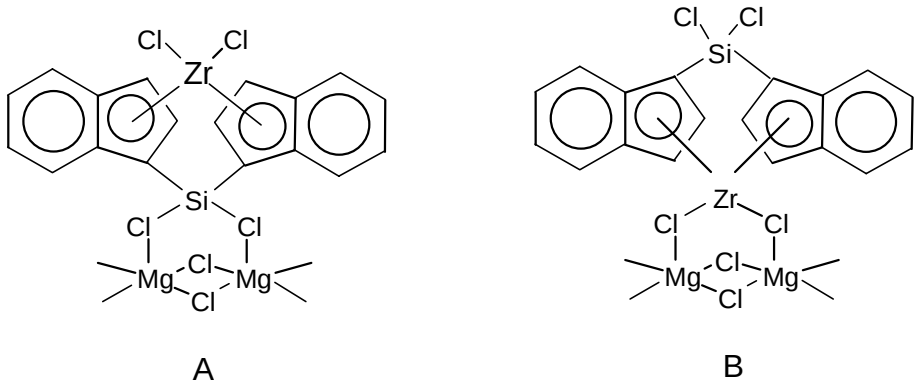

Figure 6 Possible surface binding modes for $(Cl_2Si(Ind)_2)ZrCl_2$ on $MgCl_2$

In another report, $iPr(Flu)(Cp)ZrCl_2$ and $Cp_2Zr_2Cl_2$ are supported on Al_2O_3 and $MgCl_2$ and activated by $Al(CH_3)_3$. The catalysts polymerize propylene with activities ranging from 167 kg PP/mol Zr •h for Al_2O_3 to 152 kg PP/mol Zr •h for $MgCl_2$.[27] Similar results for polyethylene are obtained using Cp_2TiCl_2 on $MgCl_2$ with TIBAL (triisobutylaluminum) as the activator.[28] Sensarma also supports Cp_2TiCl_2 and Cp_2ZrCl_2 onto $MgCl_2$ giving catalysts which polymerize ethylene at rates of ~ 200 kg PE/mol Ti• hr.[29,33]

Marks and coworkers anchor $Cp_2Zr(CH_3)_2$ onto various sulfated zirconia surfaces and obtain ethylene polymerization activities ranging from 1.5 to 40 kg PE/ mol Zr•hr.[34] Chien and Hsieh react Cp_2ZrMe_2 and $CpTiMe_3$ with Mg(OH)Cl to form a mixed catalyst which polymerizes propylene albeit with low activity.[8] Still other inorganic surfaces have been investigated but have not resulted in important heterogeneous catalysts systems with direct applicability in industrial processes.

1.4.2 Molecular Support Models

Silsequioxanes $[((C_6H_{11})_7Si_7O_9)(OH)_3]$ serve as "supports" for single-site catalysts. Buys and coworkers obtain the products shown in Figure 7 from the reaction of Cp_2TiCl_2 and $CpTiCl_3$ with the indicated support. The resulting species are inactive in PE polymerization even after

treatment with MAO.[35] They postulate that the silsequioxane they used reacts differently than a silica surface does with titanocenes and is therefore is a poor model for investigating silica surface reactivity.[35]

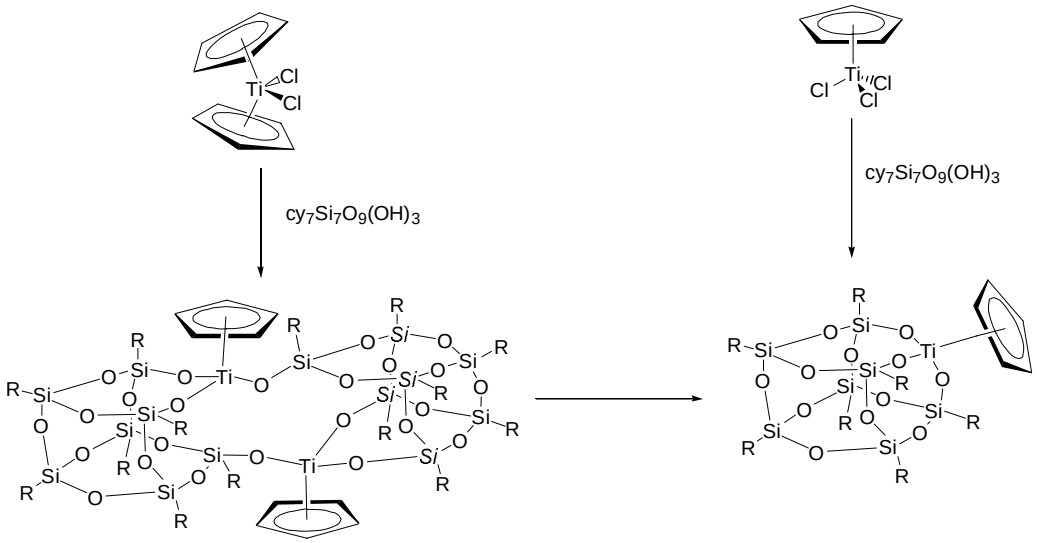

Figure 7 Products for reaction of Cp_2TiCl_2 and $CpTiCl_3$ with $((C_6H_{11})_7Si_7O_9)(OH)_3$

R. Duchateau and coworkers use mono-lithiated cuboctameric silsesquioxane (c-$C_5H_9)Si_8O_{12}Li$ as a support and obtain the product shown in Figure 8. Following activation with MAO they can polymerize ethylene, albeit with low activities (5.7 kg PE/mol Ti· •hr).[36] The purpose of their research is to develop a soluble model system for silica-grafted olefin polymerization catalysts.[36]

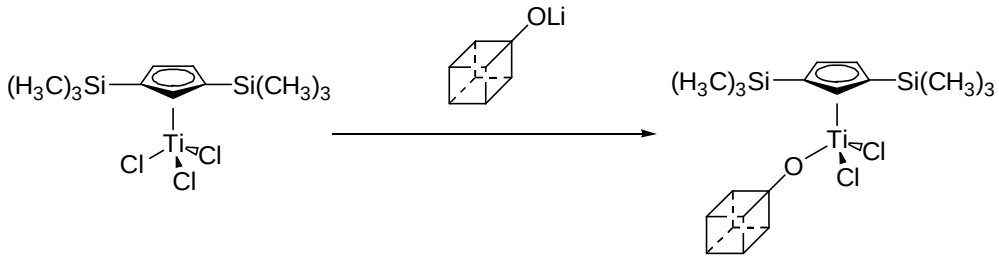

Figure 8 Products for the reaction of $((CH_3)_3Si)_2CpTiCl_3$ with mono-lithiated silsequioxane

1.4.3 Organic Support Surfaces

Soga and coworkers support rac-($Ph_2Si(Ind)_2$)$ZrCl_2$ on cross linked polystyrene beads. Scheme 2 illustrates the stepwise immobilization of the metallocene.

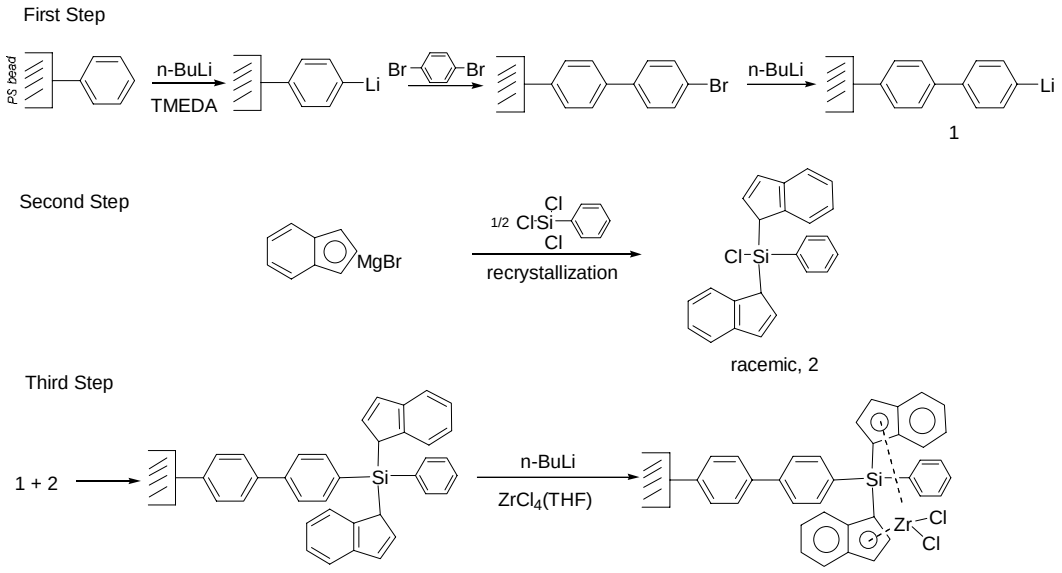

Scheme 2

The ethylene polymerization activity at 40 ^{o}C and Al/Zr molar ratio of 5000 is 9840 kg PE/mol Zr•h.[37] Unlike other immobilized metallocenes, the activity of this catalyst increases up to 150 ^{0}C at which point it is also thermally stable even though the spherical polyethylene bead shape disappears.[37] A different approach builds the catalysts into a crosslinked polystyrene matrix as illustrated in Scheme 3. The catalyst polymerizes ethylene and propylene in slurry processes. This approach avoids polar components on the support surface that could decrease the catalyst activity.[38]

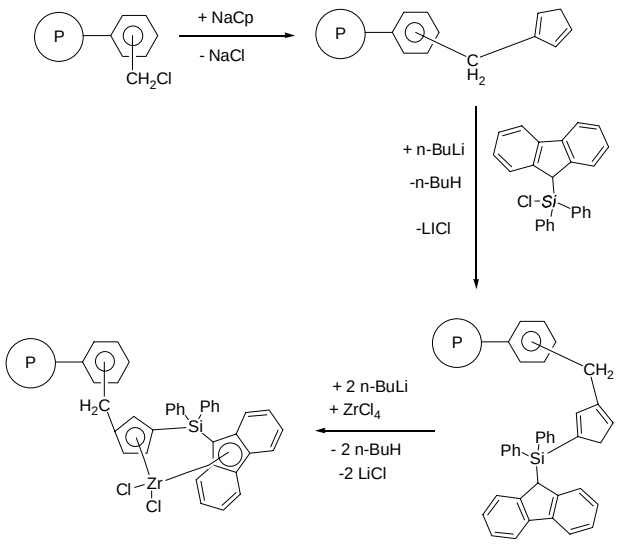

Scheme 3

A variation of the polymer support surface is the use of polysiloxanes as heterogenization media. Soga reports the synthesis of polysiloxane supported bis(indenyl), bis(fluorenyl) and bis(1,2,3,4-tetramethylcyclopentadienyl) zirconium dichloride catalysts.[39] The supported metallocene (Scheme 4) is synthesized by the hydrolytic condensation of SiH_2Cl_2 and any of the above ligands. The intermediate then reacts with $ZrCl_4$•2THF complex. Ethylene polymerization activities range from 65 to 7880 kg PE/ mol Zr•hr with an Al/Zr ratio of 5000 at a temperature of 40 ^oC, which rival the homogeneous analogues and the catalytic species is claimed to be more stable than the homogeneous catalytic species.[39] Soga emphasizes that by building indenyl and flourenyl functionalities into his polysiloxanes he can control surface structure which is a major problem in silica supported catalysts. Other research groups use different synthetic methods with polysiloxanes and obtain similar activities with structurally similar supported zirconocenes.[40,41]

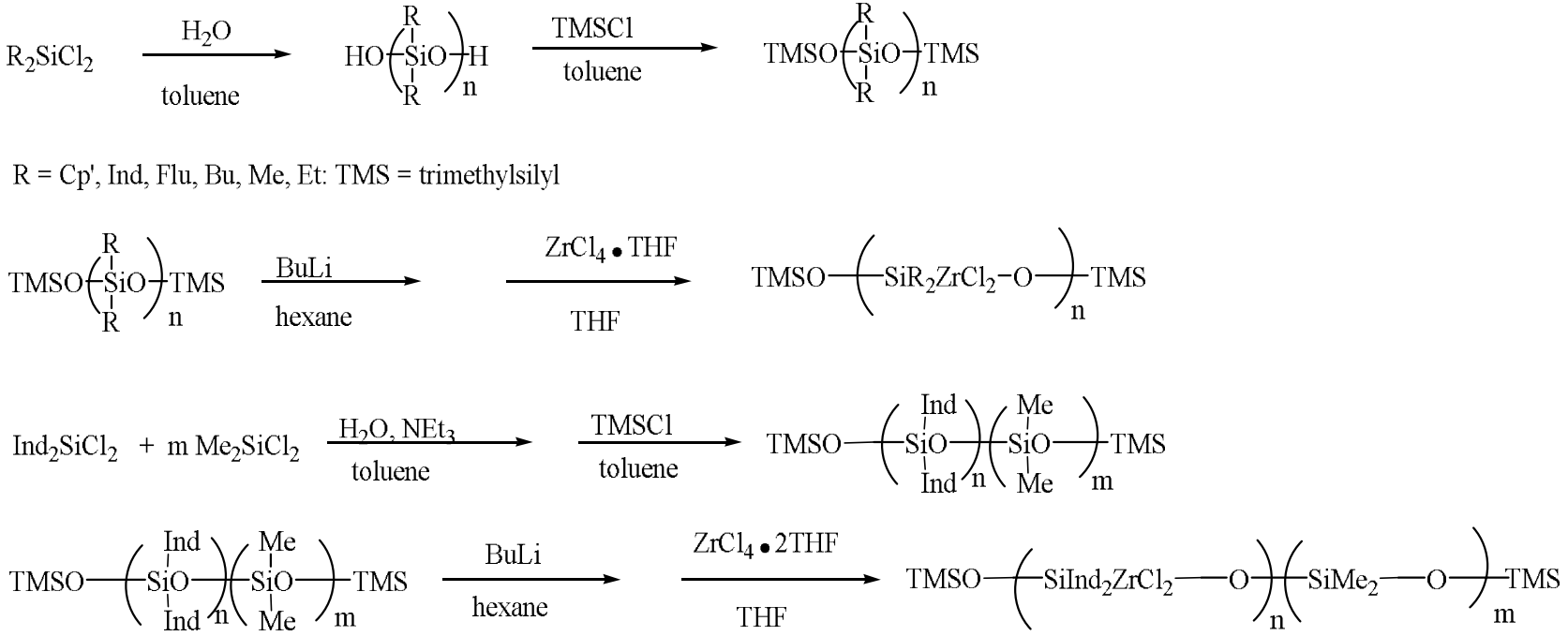
R2SiCl2
H2O
toluene
HO
SiO
H
n
TMSCl
toluene
TMSO
TMS
R = Cp', Ind, Flu, Bu, Me, Et: TMS = trimethylsilyl
BuLi
hexane
ZrCl4 • THF
THF
SiR2ZrCl2
Ind2SiCl2 + m Me2SiCl2
H2O, NEt3
Ind
Me
SiIn d2ZrCl2
SiMe2

Scheme 4

1.4.4 Silica Support Surfaces

Because of the importance of silica for our ultimate goals, prior studies of silica-immobilized metallocenes and the various methods for immobilizing metallocenes on silica are examined in this section. Section 1.4.5 describes some characteristics of silica, section 1.4.6 describes the study of metallocenes chemisorbed on silica, including problems that can arise, and section 1.4.7 describes a convenient "workaround" that has found some industrial applications.

1.4.5 Characteristics of Porous Silica

Just as with Ziegler-Natta catalysts, direct chemisorption of the catalyst onto silica can be problematic. The problems with silica stem from its highly variable surface structure which changes with temperature and other conditions. Silica surfaces are covered with OH groups and a layer of water. A fully hydrated surface contains 4.6 hydroxyls/nm.[42] Water can be removed by annealing the silica under vacuum at ~450 ^{o}C. Figure 9 illustrates some the three different types of OH groups on a silica surface.

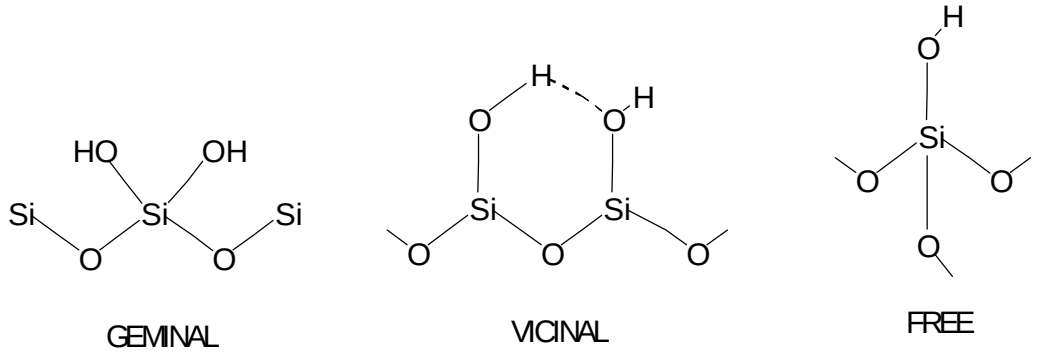

Figure 9 Types of hydroxyl groups on silica surface

Studies reveal that from 200 ^{o}C to 400 ^{o}C, dehydration is reversible. Above 400 ^{o}C rehydration is unfavored but still possible.[43] Above 850 ^{o}C there are virtually no OH groups left on the surface and the silica is hydrophobic. Sintering begins at 900 ^{o}C, and above 1200 ^{o}C there

are absolutely no silanols left.[42] The silica dehydroxylation temperature influences activity and catalyst loading. In a typical analysis the highest activity (510 kg PE/mol Zr• hr) was achieved with a dehydroxylation temperature of 450 ^{o}C and loading of 0.35 wt% Zr/SiO_2.[44] Dos Santos also found that silica surface saturation with catalyst results in a tenfold decrease in polymerization activity relative to homogeneous analogs.[45] One approach to obtaining control of surface coverage is to passivate dehydroxylated silica with several organosilicon compounds as a means of controlling catalyst loading and polymer properties.[46] The resulting polyethylenes have narrow MW distributions and activities as high as 18900 kg PE/mol Zr •h.[46]

1.4.6 Direct Adsorption

Direct immobilization of metallocenes onto silica results in active polymerization catalysts, although in many cases the activity suffers from numerous catalyst "poisoning" interactions, such as bimolecular deactivation where surface catalyst species react to form a dimeric bimetallic complex which is inactive. Direct interaction of surface hydroxyl groups can deactivate group 4 metallocenes or allow some of the catalysts to desorb from the surface during polymerization resulting in a bimodal molecular weight distribution for the polymer product.[11] One "mode" is due to the desorbed homogeneous species and the other to the heterogeneous species.

1.4.7 Alternative Approaches to Combining Metallocenes, Alumoxanes and Silica Supports

Because metallocenes are typically activated with MAO, immobilization techniques often vary the method of incorporating MAO into the catalyst system. In many cases the heterogenization process depends on the effectiveness of supporting MAO. A method pioneered by Hlatky involves immobilizing the alumoxane on silica before adding the metallocene catalyst. These systems are referred to as Alumoxane Supported catalysts.[11] Elsewhere MAO is only used

as a subsequent activator. A second approach involves premixing the metallocene and the activator (MAO) and then depositing the 'pre-activated' catalyst on silica using an incipient wetness technique.

1.4.7.1 Pre-immobilization of Alumoxane on Silica

In an effort to reduce catalyst bimolecular deactivation on a silica surface, Collins and coworkers treat dehydroxylated silica with $Al(CH_3)_3$ and subsequently support ansa-zirconocenes. Polymerization results for propylene indicate moderate activities for these supported catalysts of 689 kg PE/mol Zr·h.[47] Clearly, an alumoxane activator is still required. Welborn[48] and Takahashi[49] react a toluene/MAO solution with silica. The solvent is then volatized and the solid is collected. The silica/MAO solid is then stirred with Cp_2ZrX_2 (X= Cl, Me) in toluene. The final solid product is dried and used in gas-phase ethylene polymerizations and co-polymerizations. Other methods chemically modify the MAO when supporting onto silica. Reaction of bisphenol A (4,4'-isopropylidenediphenol) with MAO and silica in THF followed by reaction with $EBIZrCl_2$ results in a silica supported catalyst that polymerizes propylene into spherical particles.[50]

There are numerous examples in the patent literature that first support MAO onto silica and then subsequently react theses surfaces with substituted zirconocenes and hafnocenes. Targor holds several patents that use alumoxane-supported metallocenes for the synthesis of polyolefins. A particularly successful example is the Novolen process, which employs the same catalyst supporting method for the gas phase synthesis of isotactic polypropylene.[51-53] Exxon also holds a patent which uses a similar stepwise process to synthesize a supported metallocene which is used in gas phase polymerizations of alpha-olfines.[54]

1.4.7.2 Immobilization of Pre-Activated Metallocene/Alumoxane Mixtures

The second approach to alumoxane supported catalysts combines a solution of the catalyst with MAO and subsequently adds it to a silica slurry. The advantages of this method are that more active catalyst species are produced at lower Al/Zr ratios and less solvent is used in supported catalyst synthesis.[11] If the catalyst-MAO solution is allowed to stir for 18 h prior to combining with silica, the propylene polymerization activity of supported (Me_2Si(2-Me-4-PhInd)$_2$) $ZrCl_2$-MAO improves slightly.[55] Exxon holds several patents claiming that reaction of substituted metallocenes with MAO prior to immobilization onto porous silica results in effective polymerization catalysts. They use these supported metallocenes for the gas phase synthesis of polyethylene.[56-58] Another technique referred to as "incipient wetness" uses only enough volume of catalyst-MAO solution to fill the pores of the support.[59] The advantages of this technique are that the catalyst occupies the pores of the silica which improves polymer particle morphology, and that less solvent is used in catalyst preparation.[59]

1.5 Covalently Tethered Metallocenes

Covalently tethering is by far the most commonly studied method of catalyst heterogenization in academic laboratories. Tethering reduces catalyst leaching from the surface during polymerization. Leaching leads to reactor fouling. The most common techniques of tethering single-site catalysts involve reacting a substituted metallocene with reactive surface functionalities. In most cases the silica surface hydroxyls are the reactive groups and react with a substituent on the metallocene ancillary ligands to create a bond. Figure 10 illustrates the tethering idea.

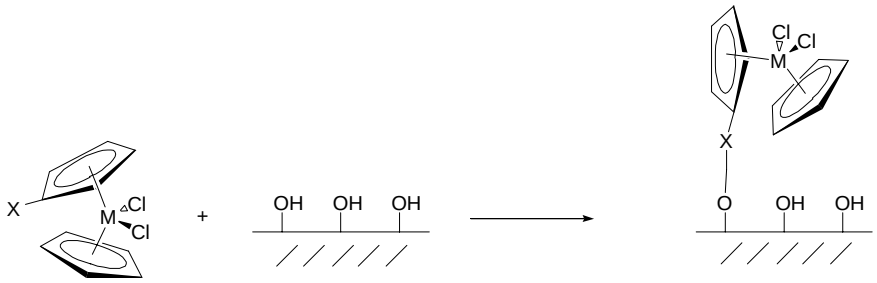

Figure 10 Chemical tethering of a functionalized metallocene to a silica surface

Lee and coworkers[60] react substituted zirconocenes (Figure 11a) with silica to produce a supported catalyst which is tethered by ether bonds (Figure 11b). The ethylene polymerization activities are lower than the homogeneous analog ($4.8x10^3$ kg PE/mol Zr•h) and are highest for an "n" value of 6.

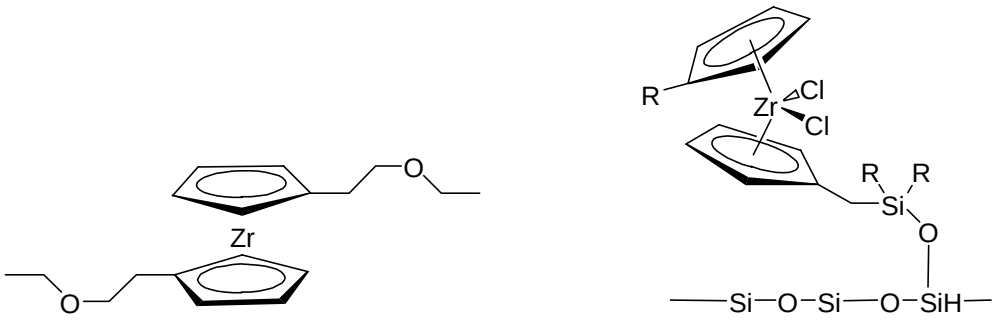

Figure 11 Tethering of substituted metallocene to silica via ether linkage

Brintzinger and coworkers react partially dehydroxylated silica (PDS) with $ClCH_2C_6H_4Si(OMe)_3$ and $Me_2Si(2\text{-}Me_2NInd)_2ZrCl_2$ to give an active propylene polymerization catalyst with an activity of 4100 kg PP/mol Zr •h (Scheme 5).[61] The advantages of Brintzinger's method as well as other chemical tethering methods is that less MAO is needed to activate the catalyst. The surface is passivated prior to addition of the catalyst, which controls surface OH reactivity and prevents "poisoning" of the catalytic species. Also, the $ClCH_2C_6H_4Si(OMe)_3$ functionality acts as a spacer unit and as a flexible anchor for the metallocene.

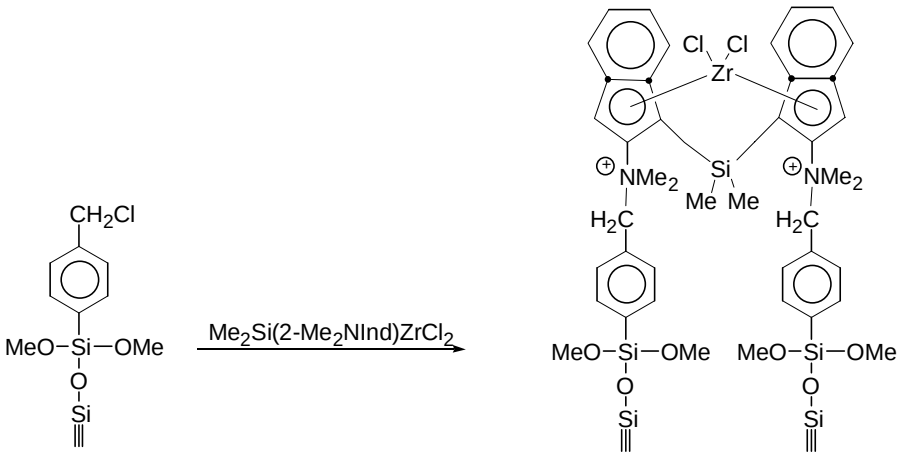

Scheme 5

Ansa-metallocenes can tether to silica via the bridging group. Reaction of $ClMeSi(Cp)_2ZrCl_2$ with PDS gives an active ethylene-1-hexene co-polymerization catalyst. Unfortunately the catalyst activity is 75% less than the homogeneous counterpart. Suzuki and coworkers tether a C_2 symmetric catalyst to silica (Figure 12). The catalyst polymerizes propylene with an activity of 4110 kg PP/mol Zr •hr atm at 60 ^oC.[62]

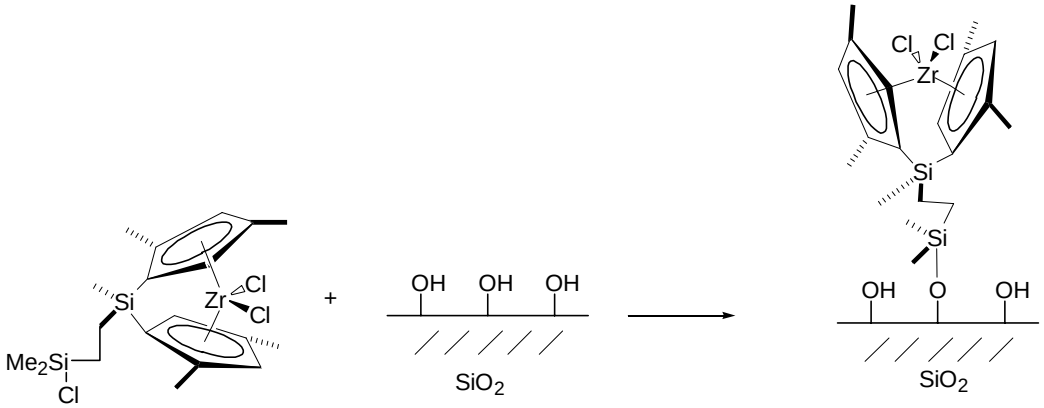

Figure 12 Tethering of ansa-metallocene to silica surface via the ansa bridge

Yet another tethering approach assembles the metallocene on the support surface. Iiskola and Pakannen react silica with $Cp(CH_2)_3Si(OCH_2CH_3)_3$ and obtain a cyclopentadienide

substituted silica surface. Subsequent lithiation and reaction with $CpZrCl_3$ affords an active ethylene polymerization catalyst.[63]

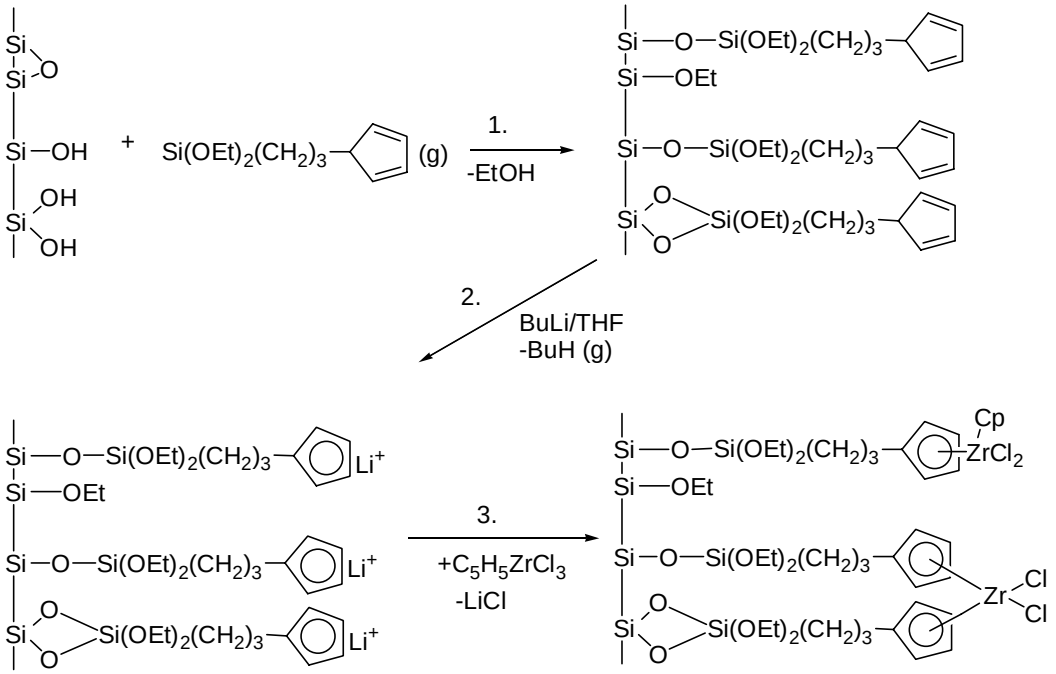

Scheme 6

One possible problem is that the tethers could "bend" and allow the metal center to contact surface OH groups and "poison" the catalytic species as illustrated in Figure 13.

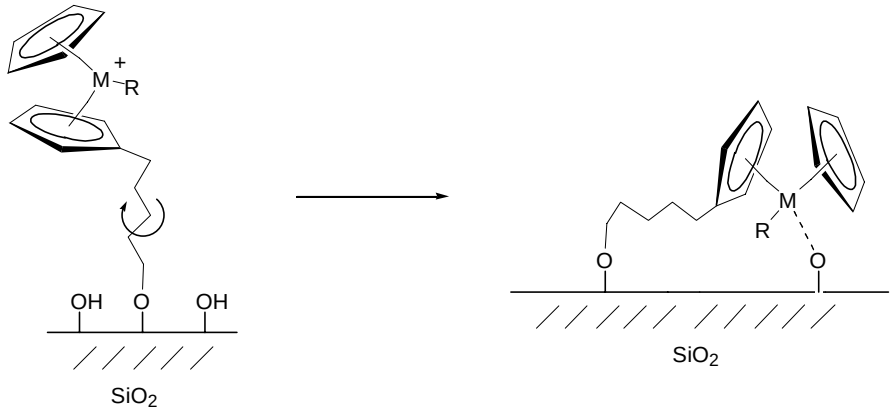

Figure 13 Illustration of long tether catalyst poisoning on silica surface

1.6 Concluding Remarks on Supported Metallocene Catalysts

Research directed toward the immobilization of single-site catalysts is varied. Understanding of single-site catalysts has come a long way since the synthesis of the first metallocene. Many challenges and problems have been encountered and addressed in catalyst heterogenization, but there are still many aspects of metallocene immobilization chemistry yet to be explored. In an effort to answer some questions concerning the structure of immobilized metallocenes and in keeping with our research objectives, we set out to model a silica surface using self-assembled monolayers.

A limited number of reports in the literature discuss efforts directed toward characterizing silica supported single-site catalysts. Lindblad and coworkers report infrared spectroscopic (IR) studies of CO stretching frequencies of silica supported cobalt and iron carbonyl complexes.[64] Iiskola and coworkers use transmission IR to characterize silica supported constrained geometry titanium catalysts.[65] Other researchers use electron paramagnetic resonance spectroscopy (EPR) to also characterize immobilized metallocenes[66] and half-metallocenes[67] on silica. They all meet with some success, but none is able to establish direct relationships between surface metallocene structure, polymerization activities and resulting polymer properties. This difficulty in surface species characterization is due to difficulties associated with spectroscopically characterizing silica. Silica is an amorphous material and, unless a single crystal is used, it is exceedingly difficult to use IR or any other type of reflectance spectroscopy to identify surface bound species.

Fisher, Downey, and Deck reported the synthesis of a series of bromodimethylsilyl substituted metallocenes from trimethylsilyl substituted precursors.[68] This B-Si exchange reaction is selective, replacing only one CH_3 group on each $SiMe_3$ moiety. As mentioned before,

several research reports claim to immobilize metallocenes onto silica via long chain ancillary ligand tethers.

Unlike the long tethers, the bromodimethyl substituted metallocenes provide an alternative short tether anchoring system. It is known that the Br is labile and reacts with nucleophiles easily. Scheme 7 shows the products of the reaction of catechol and of water with these substituted complexes.

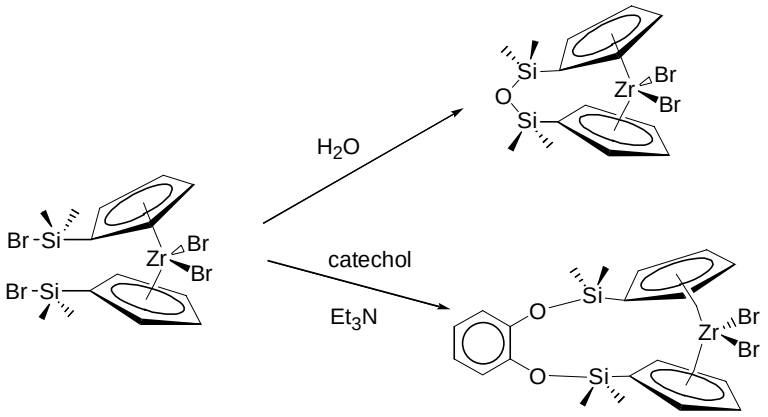

Scheme 7

The reaction with catechol works well because the interhydroxyl distance is fixed and short (~2.7 Å). Achieving even spacing of surface functionality in the case of silica is difficult. On fully hydroxylated silica the average interhydroxyl distance is 4.6 Å. This problem can be circumvented by using self-assembled monolayers of alkanethiolates on gold. Thiols self assemble on gold surfaces and form well-ordered structures. Most importantly, SAMS lend themselves to spectroscopic characterization by IR, X-ray photoelectron spectroscopy (XPS), and surface-enhanced raman spectroscopy (SERS).

In order to characterize a molecule on a surface, the structure of the compound being immobilized must be well characterized. More importantly, the immobilization surface structure must be known. Silica is an amorphous material, which makes characterization by

conventional spectroscopic techniques difficult. In order to model a silica surface, the model must have similar surface functionality and surface chemistry. The immobilization surface structure should be easily controllable and characterizable by surface spectroscopic techniques. Hydroxyl terminated self-assembled monolayers were chosen as the immobilization medium because they meet the aforementioned requirements for a model surface.

1.7 Self-Assembled Monolayers

Self-assembled monolayers (SAMs) are ordered molecular assemblies formed by the adsorption of an active surfactant on a solid support.[69] SAMs are highly ordered and uniformly oriented. They are typically composed of alkyl chains which can incorporate numerous functionalities at the chain termini, allowing access to many chemically tailored surfaces.[69] Due to their dense and stable structures, SAMs have potential applications in corrosion protection, chemical and biochemical and other technological applications. Most of the recent reviews deal with SAMs on gold surfaces, which are the best understood SAMs to date.[70-73]

1.8 Methods for Preparing Monolayers

Self-assembled monolayers can be prepared by two distinct methods. One is the Langmuir-Blodgett approach which spreads an amphiphilic molecule on water. Subsequent dipping of a substrate into the water places a layer of the amphiphilic molecule on the substrate surface. With the Langmuir-Blodgett method, the deposited layer must be compressed prior to deposition.[74] When the second "self-assembled" method of monolayer preparation was developed, scientists began to find more applications for self-assembly. The SAM forms because of strong metal-head group interactions and strong Van der Waals and dipole-dipole interactions between alkane chains which order with gauche defects between adjacent molecular chains on the substrate surface [69] allowing for hexagonal close-packing of hydrocarbon chains.

Figure 14 illustrates a monolayer on a substrate and the dense packing and ordering associated with SAMs.

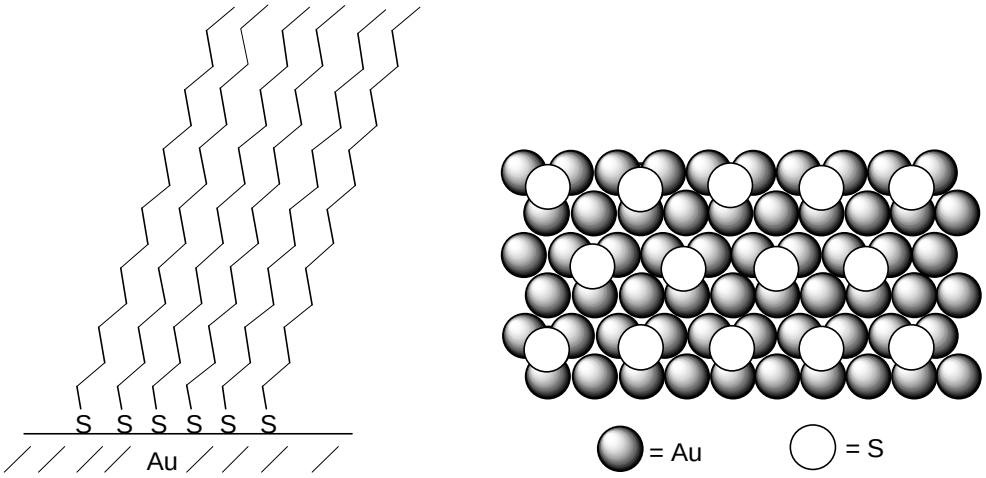

Figure 14

The diagram at left illustrates a side view of alkanethiolates on gold. The diagram at right illustrates a top view of an epitaxial hexagonal coverage scheme for alkanethiolates on gold

1.9 Substrates Used for SAM Formation

Gold is the most commonly used substrate for sulfur-terminated SAM assembly.[69] The bonding of a thiolate group to a gold surface has a homolytic bond strength (S-Au) of 40 Kcal/mol.[69] On the basis of bond energies, the bonding of an alkane thiolate to gold is calculated to be –5.5 Kcal/mol. The process is exothermic and energetically favorable.[69] Polycrystalline evaporated gold films supported on other substrates such as glass, silicon or mica have been used. The thin gold films (1000-2000 Å thick) are vapor deposited on an adhesive layer of chromium or titanium (50-100 Å).[74] Other metal substrates have been used for thiol terminated SAM formation of which the most prominent are platinum, silver and copper. Unlike gold, these metals form a surface oxide layer which must first be removed by physical or chemical methods (etching, sputtering, or polishing) to obtain a clean, roughened surface for self-assembly to take place.[69] Because gold does not have any known stable oxides, gold substrates may be cleaned

with various strongly oxidizing solutions such as "piranha" solution (1:3 mixture of 30% H_2O_2 and concentrated H_2SO_4).[74] Alternative physical cleaning methods that are used include an oxygen plasma or ozone.[74] Cleaning of gold substrates is carried out to remove any adventitiously adsorbed materials which can interfere with SAM formation or structure.[74]

1.10 Deposition of Monolayers on Gold

Self-assembly of monolayers usually involves adsorption of the thiolate from a dilute solution at room temperature. Almost any solvent can be used as long as the thiol is soluble. Long deposition times are recommended to achieve highly ordered, high-quality surfaces.[74] From millimolar solutions, disordered monolayers are deposited in a few minutes, but a few hours or even days are required to achieve densest packing and high order of the SAM. Solvent molecules or water can become trapped in the monolayer disrupting surface packing. Various annealing methods, such as heating in a gaseous ambient environment or soaking in a hot deposition solution, have been used to minimize or eliminate solvent or water molecule trapping in the monolayer.[74] Other deposition methods have been used for SAM formation but are not discussed here.

1.11 Characterization of SAMs

1.11.1 Surface Infrared Spectroscopy

Reflectance Absorbance Infrared Spectroscopy (RAIRS) is a surface spectroscopic technique frequently used to probe monolayer structure.[74] RAIRS is used to obtain a reflection spectrum of the monolayer on metal mirror surfaces such as gold. Light from an infrared source is directed onto the monolayer surface with the aid of a reflectance attachment placed in the path of the infrared beam. Figure 15 illustrates the experimental attachment necessary for surface reflection IR spectroscopy.

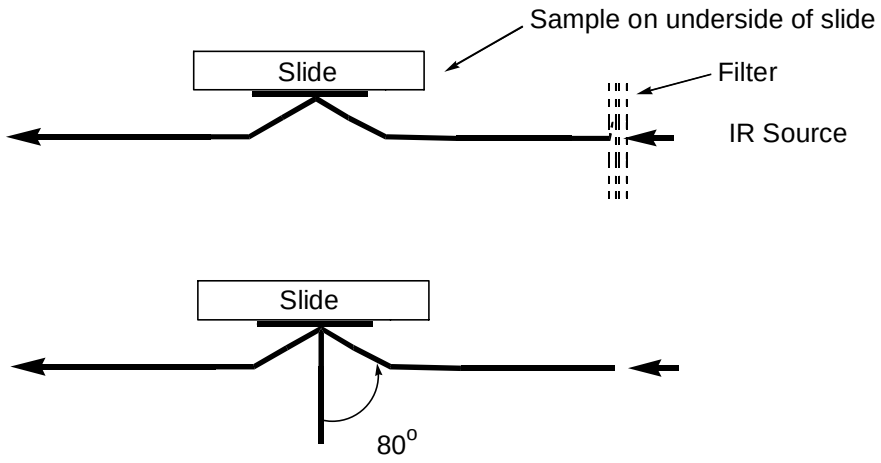

Figure 15

Reflection attachment that directs light onto sample surface and reflected light to the detector

According to Greenler's experiments the reflection angle is important to obtain a reflection spectrum. The component of the electric field vector normal to the surface will excite a dipole-active vibration of a molecule on the surface.[75] Greenler's conclusion gives rise to a "surface selection rule": Only vibrations having a transition dipole moment component perpendicular to the substrate surface will be active. He also showed that vibrational excitation is only likely to occur at high incidence angles, and therefore grazing angles must be used to obtain surface spectra.[75]

Greenler also found that only p-polarized radiation will excite a transition dipole moment. P-polarized radiation has its electric field vector parallel to the plane of incidence. Upon reflection, p-polarized radiation adds vectorially to its emitted vector. On the other hand s-polarized radiation, when reflected, does not vectorially add to its emitted vector. The incident vector due to s-polarized radiation is perpendicular to the angle of incidence of radiation and when reflected is phase shifted 180^{o}.[75] This phase shift is important because only transition dipole moments of "A" symmetry can produce an IR active signal and therefore only transition dipole moments that are perpendicular to the surface can interact with incident radiation and

consequently only with p-polarized light.[75] Figure 16 illustrates the interaction of s an p-polarized light with a reflection plane. Greenler's findings combined with group theoretical principles significantly limit the types of surface bound molecules that can give an IR spectrum and even more so the types of vibrations observed in the IR spectrum.

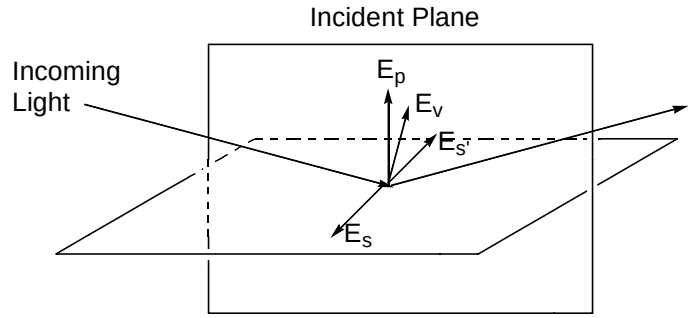

Figure 16

Schematic definition of s and p polarized light. S polarized light's E field is parallel to reflection surface (E_s and $E_{s'}$). P polarized light's E field is perpendicular to the reflection plane (E_p). The E field of a vibration (Ev) can only couple to the E field of p polarized light

Combining the surface selection rule with experimental signal intensities, the orientation of the organic molecules composing the SAM can be determined with respect to the substrate surface.

1.11.2 Surface Acidity Measurements

The most commonly used method to measure surface acidity is the sessile drop contact angle method.[74] The method involves placing a drop of aqueous or non-aqueous solutions of varying pH on the surface in question and measuring the advancing contact angle goiniometrically. The measurements are performed when drop thermodynamic equilibrium has been reached. The contact angle is the tangential angle at the point of contact of the drop with the substrate. The larger the contact angle the more hydrophobic a surface is the lower the contact angle the more hydrophilic the surface is. Figure 17 illustrates the sessile drop contact angle measurement.

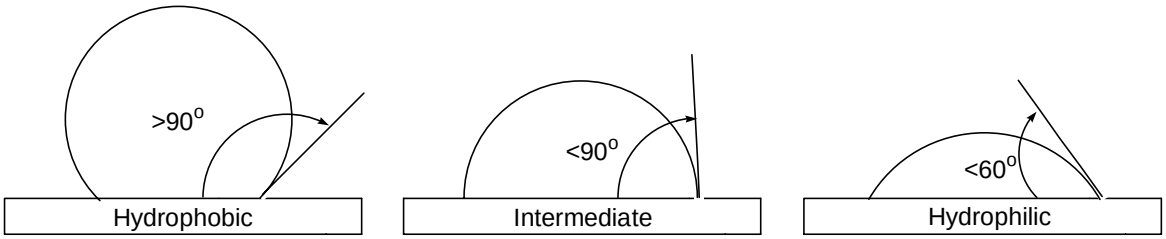

Figure 17 Illustration of contact angle measurements of different surfaces

There are also spectroscopic methods that are used to measure surface acidity, but these are not covered here.

The previous section discussing the properties of SAMs and how SAM surfaces can be characterized by various spectroscopic and physical methods emphasizes the point that SAMs are the ideal tool for modelling a silica surface and that through the use of various spectroscopic techniques a set of "fingerprints" can be developed to then characterize a surface immobilized metallocene. It is our hope that spectroscopic information will provide us with an understanding of the surface structure of a heterogeneous catalyst and eventually lead us to establish structure-property relationships for a heterogeneous single-site catalyst system.

Chapter 2

2.1 INTRODUCTION

In order to use a SAM as a model for silica, we designed a series of monolayers which would, in principle, behave like a silica surface with regard to surface functionality and acidity. Section 2.2 shows how we developed our design and which structural features of the SAM we could systematically vary. Section 2.3 and 2.4 describes the synthesis of each of our target compounds. Sections 2.5 and 2.6 detail how SAMs of compounds **1**, **2**, and **3** were prepared and functionalized.

2.2 Monolayer Design Features

The design of our "silica model" was simply a long-chain thiol terminated in a hydroxyl group. Figure 18 illustrates the general template that was used in our design. Each of the labeled components can be varied systematically. The length of the alkyl chain can be adjusted and with 12 or more carbons the resulting SAMs are expected to be more ordered. The linker "L" can be -CH_2-, -O-, or –NH- and can vary the orientation of the terminal groups or engage in hydrogen bonding affecting surface packing and SAM ordering.

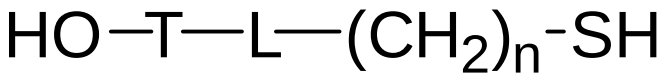

Figure 18 Template used for designing SAM surfaces

The terminal group (T) can also be varied. With T= CH_2, steric effects are, in principle, minimized, while surface ordering and packing are maximized. With T= phenylene, side reactions can be prevented. With a CH_2 group, acid catalyzed SN2 reactions with HX can occur, but with a phenylene this is not possible. The position of the OH group "T" can be para or meta

to the alkyl chain. Other substituents can be incorporated onto the arene ring and serve as additional spectroscopic "handles" or alter the manner in which the surface groups pack.

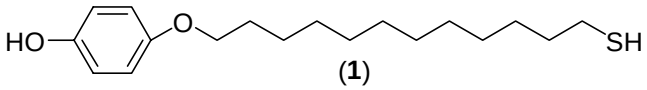

(**1**)

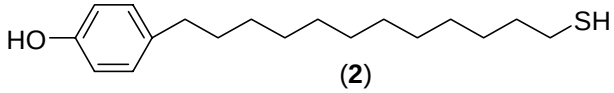

(**2**)

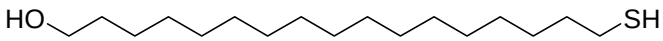

(**3**)

Figure 19 Structures of compounds 1, 2, and 3

Of many possible embodiments of the general template, **1-3** (Figure 19) were the easiest to prepare from commercially available starting materials. Sections 2.2 and 2.3 detail the results and provide a discussion of the synthetic strategy and experimental details used to obtain compounds **1**, **2**, and **3**.

2.3 Results and Discussion

The syntheses of compounds 1, 2, and 3 will be described in Sections 2.3.1, 2.3.2, and 2.3.3, respectively.

2.3.1 Synthesis of 4-(12-mercaptododecyloxy)phenol (**1**)

The first step in the synthetic scheme shown in Figure 20 involves the coupling of hydroquinone with 1,12-dibromododecane to establish the O-C linkage.

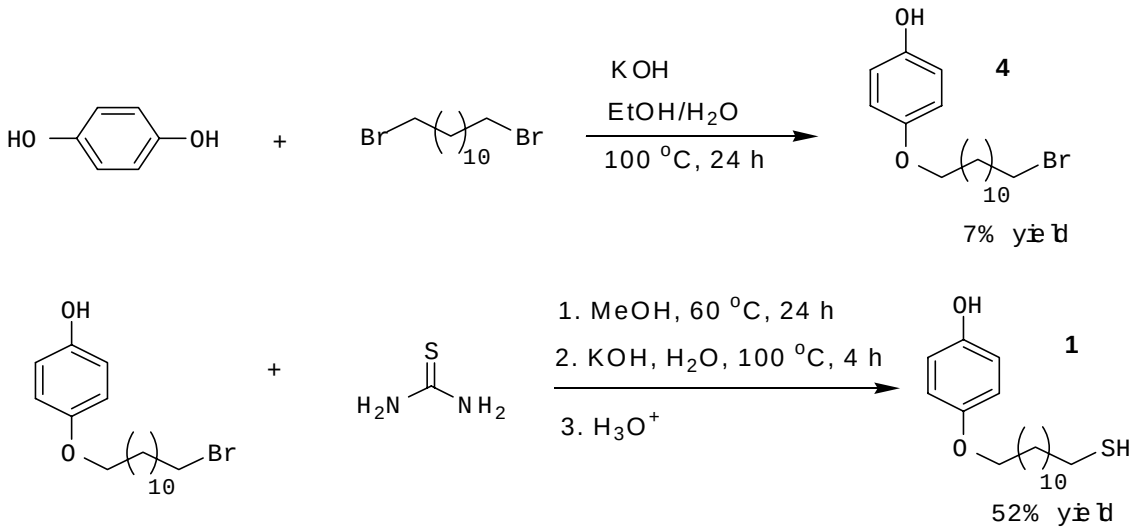

Figure 20 Synthetic scheme for compound 1

Subsequently the intermediate pendant alkyl bromide (**4**) is converted to the corresponding mercaptan (**1**). The yield for the first step was 7%. Starting materials were obtained following the purification of compound (**4**) with flash column chromatography indicating an incomplete reaction. Side reactions and byproducts (e.g., A in Figure 21) could also account for the low isolated yields. The identity of (**4**) was established by ^{1}H NMR.

The yield for the final step was 54 % and again here byproducts from incomplete alkaline hydrolysis (e.g., B in Figure 21) could account for the reduced yields. The identity of (**1**) was established by ^{1}H NMR, ^{13}C NMR and HRMS. Below (Figure 21) are some of the byproducts that could account for low yields in the synthesis of (1). Neither was isolated or observed.

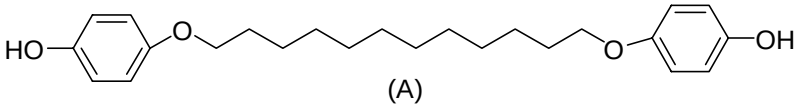

(A)

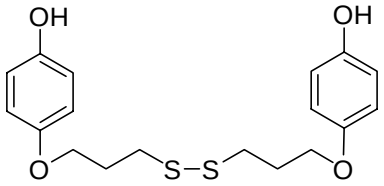

(B)

Figure 21

(A) one possible coupling byproduct from first reaction step. (B) possible byproduct from incomplete alkaline hydrolysis in the final reaction step

2.3.2 Synthesis of 4-(12-mercaptododecyl)phenol

The first step in the synthesis of compound **2** involves the lithiation of 4-bromoanisole followed by coupling with 1,12-dibromododecane to establish the $–CH_2-$ linkage as shown in Figure 22. Compound (**5**) and 4-bromoanisole could not be separated using flash column chromatography (as determined by TLC) so the product mixture was carried on to the following step. Conversion of the methyl ether to the phenol product allowed better separation of products, and compound (**6**) was obtained following separation by flash column chromatography and characterized using ^1H NMR.

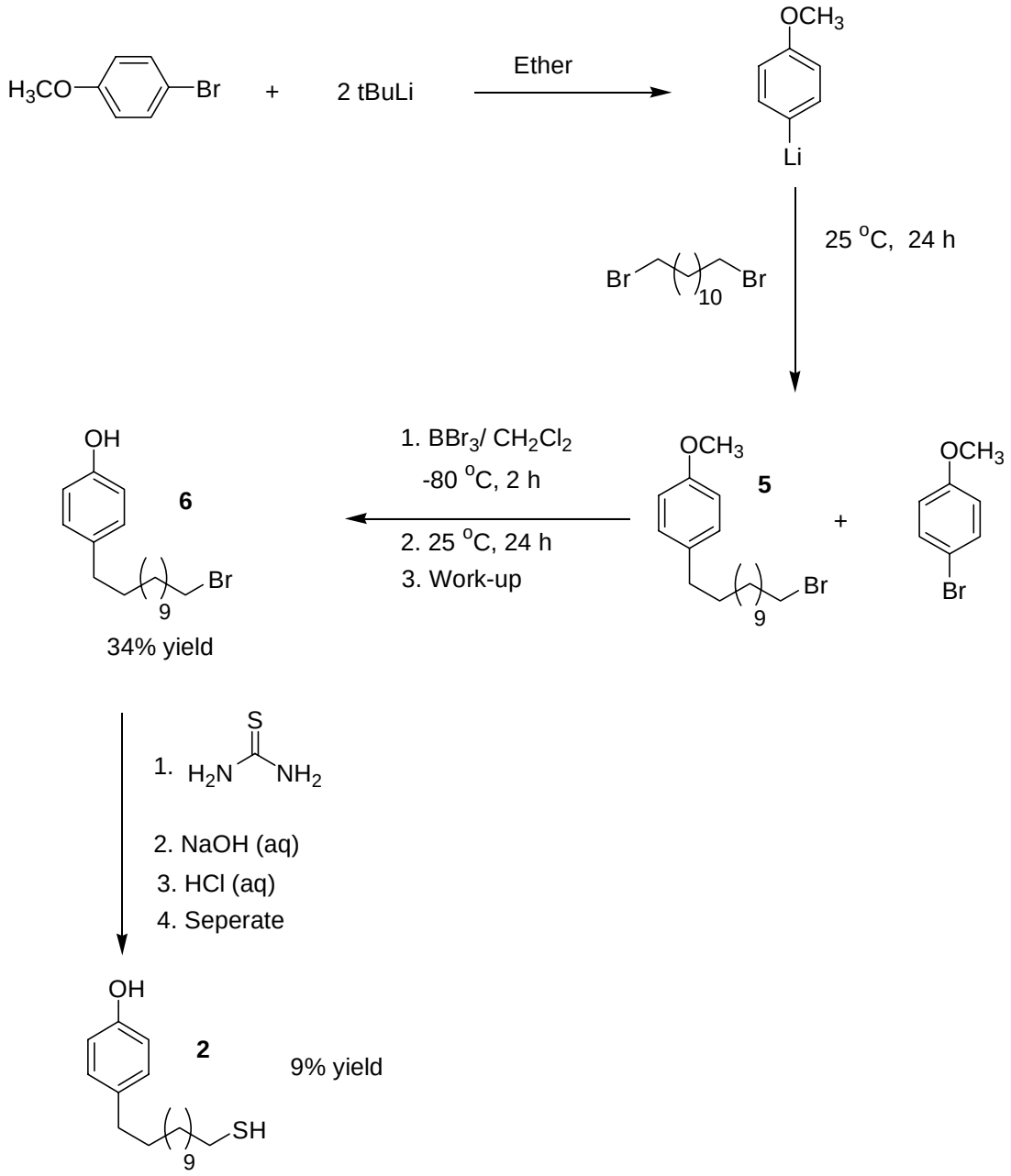

Figure 22 Synthetic scheme for the synthesis of (2)

As in the case of compound (**1**), the yields for each of the intermediate (**5**,**6**) and final products (**2**) were low and likely due to analogous side reactions resulting in byproducts structurally similar to those shown in Figure 21.

2.3.3 Synthesis of 16-mercaptohexadecanol (**3**)

The synthesis of compound **3** was greatly simplified because 16-mercaptohexadecanoic acid was commercially available. Figure 23 illustrates the synthesis.

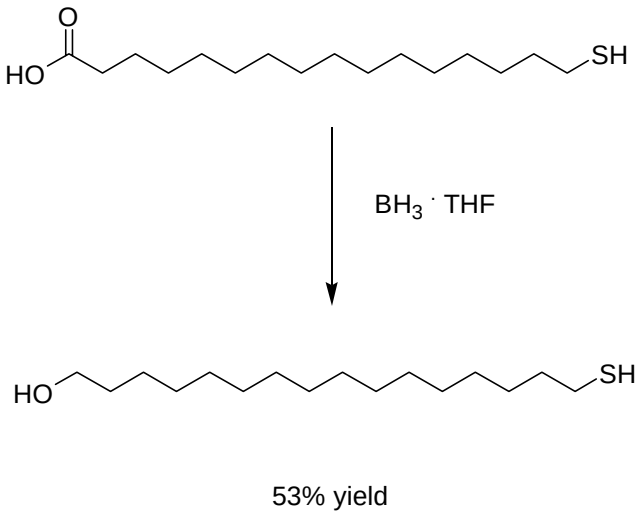

Figure 23 Synthesis of 16-mercaptohexadecanol (3)

The products of the reaction were separated using flash column chromatography. Compound (**3**) was characterized by ^{1}H NMR, ^{13}C NMR and HRMS.

2.4 Experimental Section

2.4.1 General Synthetic Methods

Hydroquinone, 1,12-dibromododecane, 4-bromo-anisole, tert-butyllithium in hexane, thiourea, 16-mercaptohexadecanoic acid, phenyl-dimethylchlorosilane, BBr_3 and BH_3 in THF were used as received from Aldrich. Potassium hydroxide, sodium hydroxide, and anhydrous magnesium sulfate were obtained from Mallinckrodt and used as received. HPLC grade ether, THF, and dichloromethane were obtained from Aldrich and were dried with an alumina column and degassed prior to use.[76] Triethylamine was obtained from Aldrich and distilled from calcium

hydride prior to use. All reactions were carried out under a nitrogen atmosphere using standard Schlenk techniques. NMR spectra were obtained on a JEOL Eclipse 500 MHz spectrometer. High resolution mass spectra were obtained on a JEOL HX100 spectrometer.

2.4.2 Synthesis of 12-(bromododecyloxy)phenol

Hydroquinone (15.0 g, 0.136 mol) was dissolved in ethanol (75 mL) in a 200 mL schlenk flask under nitrogen. A solution of 1,12-dibromododecane (10.0 g, 0.0305 mol) in 100 mL of deoxygenated ethanol was added using a syringe. A condenser was fitted, and the mixture was stirred and refluxed for 1 h under nitrogen. KOH (2.22 g, 0.0396 mol) was added to the mixture, and the reaction was refluxed overnight. The solvent was then evaporated. The product (crude **4**) was collected and dissolved in 100 mL of benzene. The solution was refluxed overnight using a Dean-Stark apparatus to remove water. Benzene was then evaporated and the white solid placed in the thimble of a Soxhlet apparatus and extracted with pentane. After evaporation of the pentane, NMR analysis confirmed a complex mixture of products which was then separated using flash chromatography on silica gel, eluting with, 10% ethyl acetate in hexane. NMR analysis confirmed the identity of the desired intermediate. 0.70 g (7% yield) of the brominated product (**4**) was obtained. ^{1}H NMR ($CDCl_3$, 400 MHz): 1.27 (m, 16H, -$(CH_2)_8$-), 1.72 (p, 2H, -($\underline{CH_2}$-CH_2-OPh)), 1.49 (p, 2H, ($\underline{CH_2}$-CH_2Br)), 3.40 (t, 2H, $\underline{CH_2}$Br), 3.84 (t, 2H, $\underline{CH_2}$-OPh), 4.33 (s, 1H, -O$\underline{H}$), 6.77 (m, 4H, Ph).

2.4.3 Synthesis of 12-(mercaptododceyloxy)phenol

The intermediate alkyl bromide (**4**, 0.70 g, 0.00196 mol) was dissolved in 50 mL of deoxygenated methanol in a 100 mL Schlenk flask under nitrogen. A solution of thiourea (0.72 g, 0.00947 mol) in methanol (25 mL) was added by syringe. The resulting solution was heated under reflux for 24 h. Methanol was then evaporated, and a white solid was collected. The solid

was dissolved in 100 mL of 2M aqueous NaOH and refluxed for 4 h. 2 M aqueous HCl was then added to acidify the product mixture. The mixture was then extracted with hexane for 48 h using a continuous liquid-liquid extraction apparatus. The collected hexane was then evaporated to afford a crystalline white solid (crude **1**). The compound was then purified using flash chromatography on silica gel, eluting with 10% ethyl acetate in hexane. The thiol was obtained in a 52 % yield (0.312 g, 0.0010 mol) as a crystalline solid after evaporation of the second chromatographic fraction. ^{1}H NMR ($CDCl_3$, 500 MHz): 1.26 (m, 16H, -$(CH_2)_8$), 1.53 (s, 1H, -S<u>H</u>), 1.59 (p, 2H, -(<u>CH_2</u>-CH_2-SH)), 1.74 (p, 2H, (<u>CH_2</u>-CH_2OPh)), 2.52 (q, 2H, <u>CH_2</u>SH), 3.88 (t, 2H, <u>CH_2</u>-OPh), 6.77 (m, 4H, Ph). ^{13}C NMR (CD_2Cl_2, 500 MHz): 26.46 (<u>CH_2</u>-SH), 27.92 (CH_2), 30.27 (CH_2), 30.97 (CH_2), 31.29 (CH_2), 31.29 (CH_2), 31.29 (CH_2), 31.46 (CH_2), 31.46 (CH_2), 31.46 (CH_2), 36.04 (CH_2), 70.52 (<u>C</u>H_2-OPh), 117.33 (Ph), 117.73 (Ph), 155.27 (Ph). HR-MS m/z: 310.1935 a.m.u. Calculated m/z: 310.1967 a.m.u.

<u>2.4.4 Synthesis of 12-(bromododecyl)phenol</u>

To a solution of 3.90 g (0.021 mol) of 4-bromoanisole in 50 mL of ether in a 200 mL schlenk flask was added tert-butylithium in hexane (24.5 mL, 1.7 M, 0.0416 mol) slowly. The reaction was stirred for 1 h. Then, a solution of 1,12-dibromododecane (6.96 g, 0.0212 mol) in 50 mL of ether was added by syringe. The mixture was stirred for 24 h. After evaporating the solvents, the crude product mixture was separated using flash chromatography on silica gel, eluting with 10% ethyl acetate/hexane. The crude intermediate (a mixture of **5** and 4-bromoanisole) was dissolved in 50 mL of dichloromethane, cooled to –80 ^{o}C, and treated with BBr_3 (5.5 g, 0.0219 mol). The reaction was stirred for 2 h at –80 ^{o}C and then allowed to warm up to room temperature overnight. The reaction was then mixed with 120 mL of H_2O. The mixture was extracted with 200 mL of ether. The ether layer was then extracted with 120 mL of

2M NaOH solution. The aqueous layer was neutralized with 2M HCl and extracted with two 200 mL portions of ether. The ether layer was dried over anhydrous magnesium sulfate, filtered, and evaporated. The product mixture (1.38 g) was purified using flash chromatography on silica gel, eluting with 10% ethyl acetate/hexane as before. The first fraction contained compound (**6**) (7.14 g, 0.00714 mol) in 34% yield. ^{1}H NMR (CD_2Cl_2, 360 MHz): 1.28 (m, 16H, -$(CH_2)_8$-), 1.55 (p, 2H, -($\underline{CH_2}$-CH_2-Ph)), 1.85 (p, 2H, ($\underline{CH_2}$-CH_2Br)), 2.54 (t, 2H, $\underline{CH_2}$-Ph), 3.43 (t, 2H, $\underline{CH_2}$Br), 6.77 (m, 4H, Ph).

2.4.5 Synthesis of 12-(mercaptododecyl)phenol

The intermediate alkyl bromide (**6**, 2.00 g, 0.00586 mol) was treated with a solution of thiourea (1.38 g, 0.0181 mol) in 60 mL of methanol at 80 ^{o}C for 15 h. The methanol was then evaporated and treated with 150 mL of 2M KOH and refluxed for 12 h. The aqueous solution was extracted with hexane using a liquid-liquid extraction apparatus for 24 h. The hexane was then evaporated. The final product was purified using flash chromatography on silica gel, eluting with 10% ethyl acetate/hexane. The second fraction yielded 0.152 grams (9% yield) of compound (**2**). ^{1}H NMR (CD_2Cl_2, 360 MHz): 1.26 (m, 16H, -$(CH_2)_8$-), 1.55 (m, 5H, -($\underline{CH_2}$-CH_2-Ph), –($\underline{CH_2}CH_2SH$), S$\underline{H}$), 2.52 (m, 4H, (-$\underline{CH_2}$-Ph), (-$\underline{CH_2}$SH)), 4.73 (s, 1H, O$\underline{H}$), 6.71 (m, 2H, Ph), 7.02 (m, 2H, Ph). ^{13}C NMR (CD_2Cl_2, 500 MHz): 24.64 ($\underline{CH_2}$-SH), 29.20 (CH_2), 29.53 (CH_2), 29.60 (CH_2), 29.63 (CH_2), 29.64 (CH_2), 31.69 (3 CH_2), 34.02 (CH_2), 35.01 (CH_2), 35.02 (CH_2), 114.98 (Ph), 129.38 (Ph), 135.17 (Ph), 153.30 (Ph). HR-MS m/z: 294.1971 a.m.u. Calculated m/z: 294.2051.

2.4.6 Synthesis of 16-mercaptohexadecanol

To a solution of 16-mercaptohexadecanoic acid (0.40 g, 0.000138 mol) in THF (50 mL) was added 2.2 mL of a 1.0 M solution of borane in THF. After stirring for 6 h at 25 ^{o}C,

concentrated aqueous HCl solution (20 mL) was added, and the resulting mixture was stirred at 25 ^{o}C for 10 h. The solvent was evaporated, and the crude white solid product was purified using flash chromatography on silica gel, eluting with 10% ethyl acetate/ hexane. The second chromatographic fraction contained 0.200 g (0.000733 mol, 53% yield) of the desired mercaptan (**3**). ^{1}H NMR (CD_2Cl_2, 360 MHz): 1.26 (m, 24H, -$(CH_2)_8$-), 1.54 (m, 5H, -($\underline{CH_2}$-CH_2-SH), (-$\underline{CH_2}CH_2OH$), S$\underline{H}$)), 2.49 (p, 2H, $\underline{CH_2}SH$), 3.60 (t, 2H, $\underline{CH_2}OH$), 5.32 (s, 2H, O$\underline{H}$). ^{13}C NMR (CD_2Cl_2, 500 MHz): 23.65 ($\underline{CH_2}$-SH), 25.04 (CH_2), 27.61 (CH_2), 28.39 (CH_2), 28.86 (CH_2), 28.92 (7 CH_2), 28.99 (CH_2), 32.45 (CH_2), 33.28 ($\underline{C}H_2CH_2OH$), 60.61 ($\underline{C}H_2OH$). HR-MS m/z: 275.2443 a.m.u. Calculated m/z: 274.2330 am.u.

2.5 SAM Preparation

Millimolar solutions of compounds **1**, **2**, and **3** were prepared by dissolving a few milligrams of each compound in 40 ml of methylene chloride. Gold substrates were soaked in piranha solution for 5 minutes, rinsed with water and dried under an N_2 stream. The substrates were then lowered into the compound solutions and allowed to soak for 24 hours. To characterize the SAM, the slide was removed from the solution and rinsed with ethanol to remove unwanted adsorbates. The substrate was then rinsed with copious amounts of deionized water and dried under an N_2 stream.

2.6 Silanization of SAMs

SAMs formed from compounds **1**, **2**, and **3** were treated with phenyldimethylchlorosilane and triethylamine in dichloromethane. After 24 h the monolayers were rinsed with ethanol and water and dried under an N_2 stream.

Chapter 3

3.1 INTRODUCTION

Although rigorous spectroscopic characterization of the individual compounds was carried out in solution, the key surface-spectroscopic characterization measurement used to analyze the SAMs on gold substrates was RAIRS. Ultimately, we hope to use the RAIRS method to analyze metallocenes supported on the SAMs on gold substrates. These spectra will provide "fingerprint" frequencies and intensities that may be useful in analyzing infrared spectra of metallocenes supported on partially hydroxylated silica. Section 3.1.1 contains some background on the theory of RAIRS. Section 3.1.2 provides some background on DFT calculations and how we used them to assign the vibrational. Section 3.1.3 provides information concerning contact angle measurements made to estimate surface hydrophilicity. Section 3.1.4 outlines our strategy for analyzing the SAM surfaces with RAIRS.

3.1.1 Reflection-Absorption Infrared Spectroscopy (RAIRS)

RAIRS is an external reflection infrared spectroscopic technique well suited for the analysis of surface adsorbed species. The experiment relies on enhanced absorption of IR radiation, by surface adsorbed species, at high incidence angles and on the exclusive absorption of the p polarized component of the incident IR radiation. Exclusive absorption of p polarized radiation gives rise to the surface selection rule in RAIRS which states that the only active vibrations observed in RAIRS spectra must have a component of their transition dipole moment perpendicular to the surface.

The RAIRS experiment, like most modern IR experiments, uses Fourier Transform (FT) techniques. The instrumental setup is identical to a transmission FTIR instrument with the only

difference being the sample chamber where, instead of a transmission cell, a reflection attachment is used to direct the IR radiation onto the sample surface as previously illustrated in Figure 15. Resolution in RAIRS spectra is determined by the heterogeneity of the surface and the nature of the surface molecule interactions rather than any experimental limitation.[77] Surfaces which are not homogeneous in composition and structure can cause an increased signal to noise ratios which lowers resolution. Surface hydrogen bonding can "soften" C-H modes of alkanethiol SAMs on gold substrates causing broadening of the C-H bands also limiting resolution.[77]

RAIRS is an ideal technique for the characterization of SAMs because vibrational spectra can be obtained from monolayer or submonolayer quantities of surface adsorbed thiols.[77] For a given alkanethiol SAM the spectra which are obtained are simpler than the corresponding solution transmission spectra of the chosen alkanethiol, yet direct comparison of vibrational frequencies can be made between the two types of spectra. RAIRS can also provide information concerning the orientation of surface groups and the packing density of molecules on the metal substrate.[77] The disadvantage to using RAIRS is that only vibrational modes with a component of their transition dipole moment perpendicular to the surface will be observed.

RAIRS is the spectroscopic technique of choice for the analysis of SAMs of compounds **1**, **2**, and **3**.

3.1.2 Density Functional Theory Calculations (DFT)

Theoretical calculation of vibrational frequencies can aid in the characterization of new chemical compounds and guide in the assignment of normal modes observed in experimental IR spectra. There have been several reports in the literature which indicate that DFT calculational methods , predict harmonic vibrational frequencies better than Hartree-Fock methods.[78,79] The

Hartree-Fock (HF) methods consistently predict much higher vibrational frequencies on the order of 144-168 cm^{-1} depending upon which basis set is used. Using a 6-31G* basis set, HF methods calculate vibrational frequencies 168 cm^{-1} higher than experimentally observed harmonic vibrational frequencies in small molecules.[79] Using the B-LYP DFT method and a 6-31G* basis set, calculated vibrational frequencies are only 75 cm^{-1} higher than experimentally observed harmonic vibrational frequencies.[79] Although there are other DFT methods which are more accurate they are also more computationally intensive and are not included in Titan. Titan is a software program from Wavefunction, Inc. which was used to perform the DFT calculations for compounds **1**, **2**, and **3**.

Prior to calculating the vibrational modes for compounds **1**, **2**, and **3**, geometries are optimized. Titan uses a molecular mechanics minimizer which is based on the MMFF94 force field (an empirical molecular mechanics method).[80] Other geometry minimization methods are available but not included with Titan. Performing DFT calculations on compounds **1**, **2**, and **3**, using B3-LYP and a 6-31G* basis set should yield vibrational frequencies on the order of 75 cm^{-1} higher than the experimentally observed vibrational frequencies based upon previously published results.[79] Titan displays the calculated vibrational frequencies as motions of the molecule and assigns a symmetry to the mode. Many of the calculated modes can be eliminated due to their symmetry and expected intensity. Increased errors are expected in calculated values since compounds **1**, **2**, and **3** are not small molecules but the values can serve as useful guides in assigning normal vibrational modes observed in transmission IR spectra and RAIRS spectra of SAMs of **1**, **2**, and **3**.

3.1.3 Contact Angle Measurements

Contact angle measurements are widely used to measure many physical properties of surfaces. The sessile drop method is the most widely used of the various contact angle measurements.[81] The technique consists of aligning a tangent with the drop profile at the point of contact with the surface (Figure 24). Of particular interest in the characterization of SAMs is surface hydrophilicity and hydrophobicity, which can be measured using the sessile drop method.

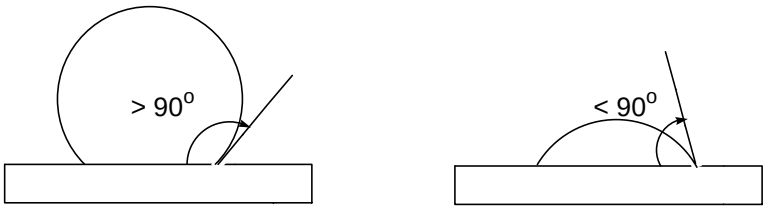

Figure 24 Examples of surfaces with contact angles greater than and less than 90°

Surfaces which are hydrophilic produce contact angles which are low (< 80°). Surfaces which are hydrophobic give high contact angles (80°-118°). Based upon the contact angles obtained, the hydrophilicity of SAMs **1**, **2**, and **3** can be measured. The values do not give absolute surface energies nor do they provide a measure of the SAMs organization.

The instrument used to measure contact angles is a goniometer. Figure 25 illustrates the components of the instrument used in the sessile drop contact angle measurement.

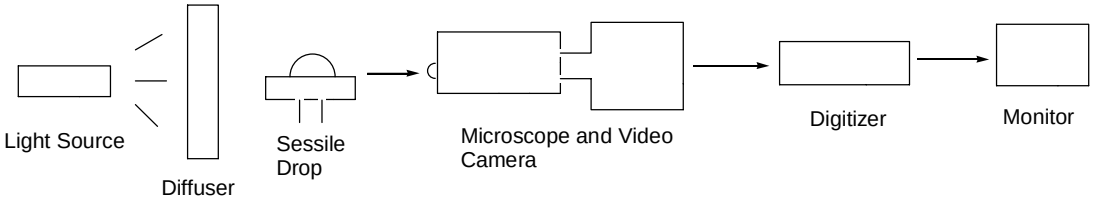

Figure 25 Components of a sessile drop goniometer

The main limitation of the sessile drop method is precision. It has been reported that differences of 10^{o}, among independent laboratories on identical surfaces, have been found.[81] Despite these possible limitations qualitative results can be extracted from the sessile drop contact angle measurement.

3.1.4 Strategy for SAM Characterization

In order to characterize each of the SAM surfaces and investigate their reactivity, several steps were followed. Transmission IR spectra for thiols **1**, **2**, and **3** were obtained followed by RAIRS spectra of SAMs **1**, **2**, and **3**. Direct comparison of transmission and reflection-absorbption IR spectra was made. Following the spectral analysis, DFT calculations on each of the three thiols was performed in order to assign the features observed in the trasmission IR spectra Frequency assignments in the RAIRS spectra was consistent with the selection rules. Following assignment of the spectra contact angle measurements of each SAM surface was performed. Each SAM surface was functionalized with phenyldimethyl-chlorosilane. RAIRS spectra were obtained for each functionalized SAM. Following RAIRS analysis contact angle measurements were performed on the silanized surfaces to asess changes in hydrophilicty of the functionalized SAMs.

3.2 DFT Calculational Results

Below are the calculated frequencies of the various vibrational modes which are expected to be observed in the IR spectra of compounds **1**, **2**, and **3**.

Vibrational Mode	Calculated Frequencies (cm^{-1})
O-H	3763
Symmetric C-H	3045, 3042, 3040, 3036, 3031,3026, 3021
Asymmetric C-H	3016, 3010, 3005, 3001
C-C Ring Modes	1793, 1786, 1680, 1623, 1594
C-O	1285, 1297, 1306, 1319

Table 1 Calculated vibrational frequencies for compound 1**.**

Vibrational Mode	Calculated Frequencies (cm^{-1})
O-H	3752
Symmetric C-H	3044, 3039, 3033, 3030, 3029, 3026, 3024, 3021
Asymmetric C-H	3016, 3014, 3011, 3010, 3008, 3007
C-C Ring Modes	1676, 1648, 1564
C-O	1308, 1305

Table 2 Calculated vibrational frequencies for compound 2**.**

Vibrational Mode	Calculated Frequencies (cm^{-1})
O-H	3755
Symmetric C-H	3041, 3038, 3036, 3035, 3031, 3030, 3027, 3026, 3022, 3020
Asymmetric C-H	3016, 3014, 3012, 3009, 3007, 3003, 3000
C-H Bending	1480
C-O	--------

Table 3 Calculated vibrational modes for compound 3.

As seen in the previous tables the values calculated for the C-H stretching modes are high relative to where these modes are expected to appear for alliphatic CH_2 groups.[82] The calculated value for the O-H stretching mode is very high relative to where O-H bands appear in IR spectra. The C-O vibrational mode for compound **3** is not distinguishable in the calculated modes and is believed to couple to the C-C stretching modes of the alkyl chain. The other calculated values fall within expected experimental error for the theoretical technique being used.

3.3 Transmission and RAIRS Spectra

Transmission IR spectra from each of the synthesized thiols and RAIRS spectra of each SAM is presented in the following subsections. Each subsection will address a different compound. The transmission and RAIRS spectra will be compared and correlated with the DFT results from section 3.2. Band assignments will be discussed and conclusions drawn about the structure of each SAM. The top spectrum of each stacked plot is the RAIRS spectrum of the indicated SAM whereas the bottom is the transmission spectrum of the corresponding thiol.

3.3.1 Transmission and RAIRS Spectra of 4-(12-bromododecyloxy)phenol (**1**)

The bottom spectrum of Figure 26 shows the transmission IR of thiol **1**. The broad feature at 3388 cm^{-1} is assigned to the terminal phenol –OH group. DFT calculations calculate the –OH stretching frequency to be 3763 cm^{-1} which is 300 cm^{-1} higher than experimentally observed values for –OH groups. The strong bands at 2849 and 2916 cm^{-1} are assigned as the symmetric and asymmetric C-H alkyl chain stretching modes, respectively. The strong band at 1515 cm^{-1} is assigned to the asymmetric stretch of the aromatic ring. The intense stretching frequency at 1240 cm-1 is assigned to the C-O stretching mode of the ether linkage and the C-O of the terminal hydroxyl group. Many other bands are observed in the transmission spectrum, but these are not observed in the surface reflectance spectrum and are therefore not assigned.

Even in well-ordered SAMs, the C-C and C-H stretches of the alkyl chain are usually not observed.[83] The assigned transmission frequencies can be correlated to the bands observed in the RAIRS spectrum of SAM (**1**) shown in figure 26. The frequency values for the C-H stretching modes from the RAIRS spectrum correspond well to the values from the transmission spectrum. The C-H stretching mode absorbances are small, which suggests the stretching mode is not coupling significantly to the incoming p-polarized radiation. The ring modes at 1515 cm^{-1} are intense and well defined, indicating a nearly perpendicular orientation of the C-O bond to the substrate surface. The stretching mode at 1241 cm^{-1} is also intense and is well correlated to the C-O mode in the transmission spectrum. The DFT calculations support the assignments which are made although the frequencies of the vibrational modes are higher than expected due to the accuracy of the calculation method employed and because compound **1** is a fairly large molecule. The deviation between calculated and experimental vibrational frequencies ranges from 45-160 cm^{-1}.

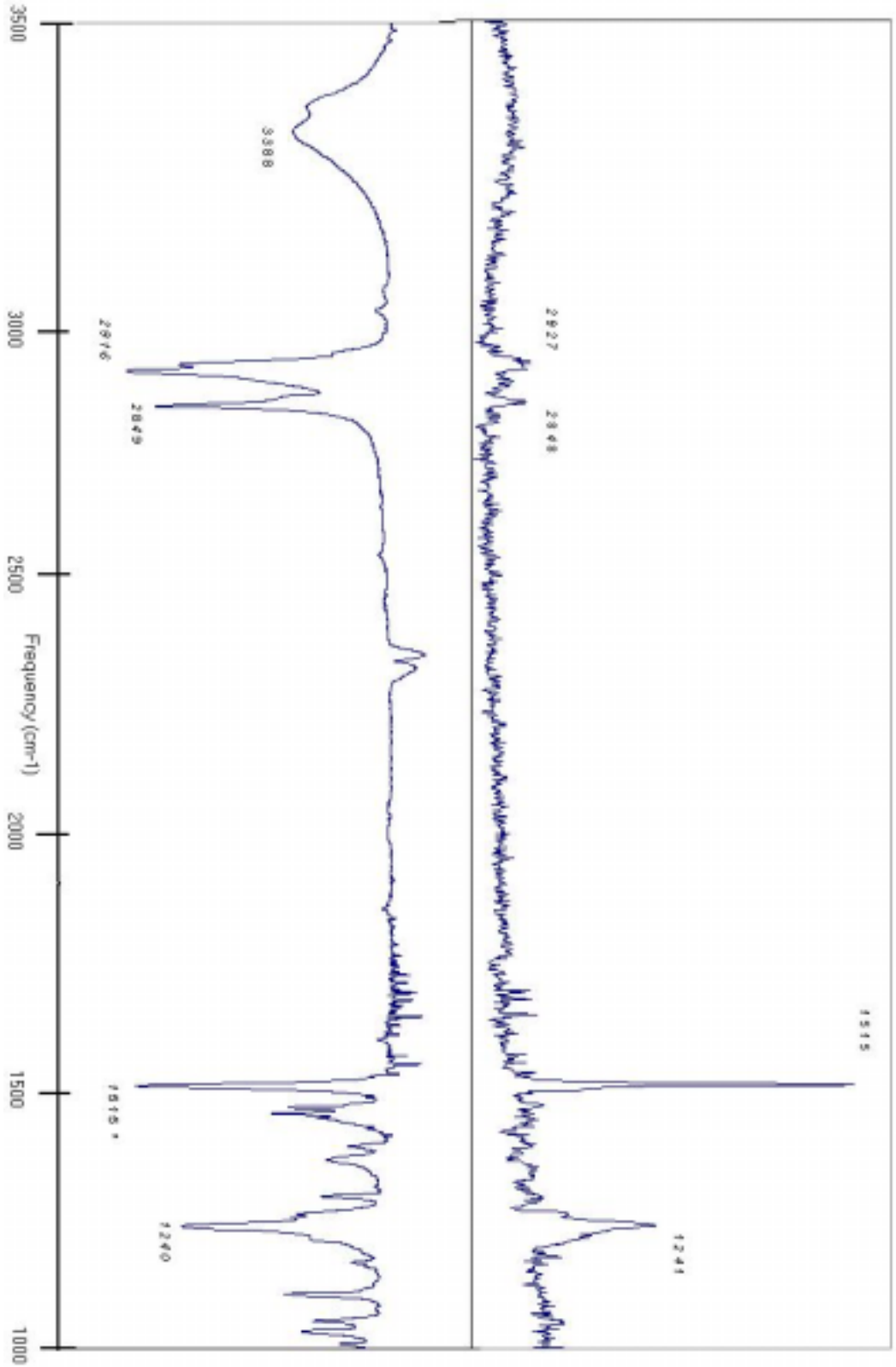

Figure 26 RAIRS and transmission spectrum of 1

3.3.2 Transmission and RAIRS spectra of 4-(12-mercaptododecyl)phenol (**2**)

The bottom spectrum of Figure 27 is the Transmission spectrum of thiol **2**. The broad feature at 3418 cm^{-1} is assigned to the terminal –OH stretching mode of the phenol. At 2919 cm-1 and 2848 cm-1 are the symmetric and asymmetric C-H stretching modes of the alkyl chain. DFT calculated values for the C-H modes are about 120 to 160 cm-1 higher than experimentally observed values. The bands at ~1600 cm^{-1}, at 1516 cm^{-1}, and at ~1460 cm^{-1} are all due to C=C ring modes and are nearly identical to those of phenol.[82] The agreement between the DFT calculations and experimental values for the C-C ring modes is better than in previously assigned modes.

The strong band at 1258 cm^{-1} is assigned to the C-O stretching mode. The peak shape and position is within 20 cm^{-1} of the C-O mode for phenol. DFT calculations predict the C-O stretching mode to be ~ 45 cm^{-1} higher than what is experimentally observed.

The top spectrum in Figure 27 is the RAIRS spectrum of SAM **2**. The bands seen at 2930 cm^{-1} and 2853 cm^{-1} are assigned to the symmetric and asymmetric C-H stretching modes respectively. The frequency values correspond well to the ones observed in the transmission spectrum. The band at 1518 cm^{-1} corresponds to a C-C ring mode and correlates well to the ring mode at 1516 cm^{-1} in the transmission spectrum. The relative absorbance values of the C-H bands and the C-C ring bands in SAM **2** are much closer than the corresponding relative absorbance values of the same peaks for SAM **1** suggesting that the alkyl chain may be more tilted in SAM **2** than in SAM **1**. The band at 1266 cm^{-1} is assigned to the C-O stretching mode of the terminal phenol and corresponds well to the value observed in the Transmission spectrum for the corresponding mode.

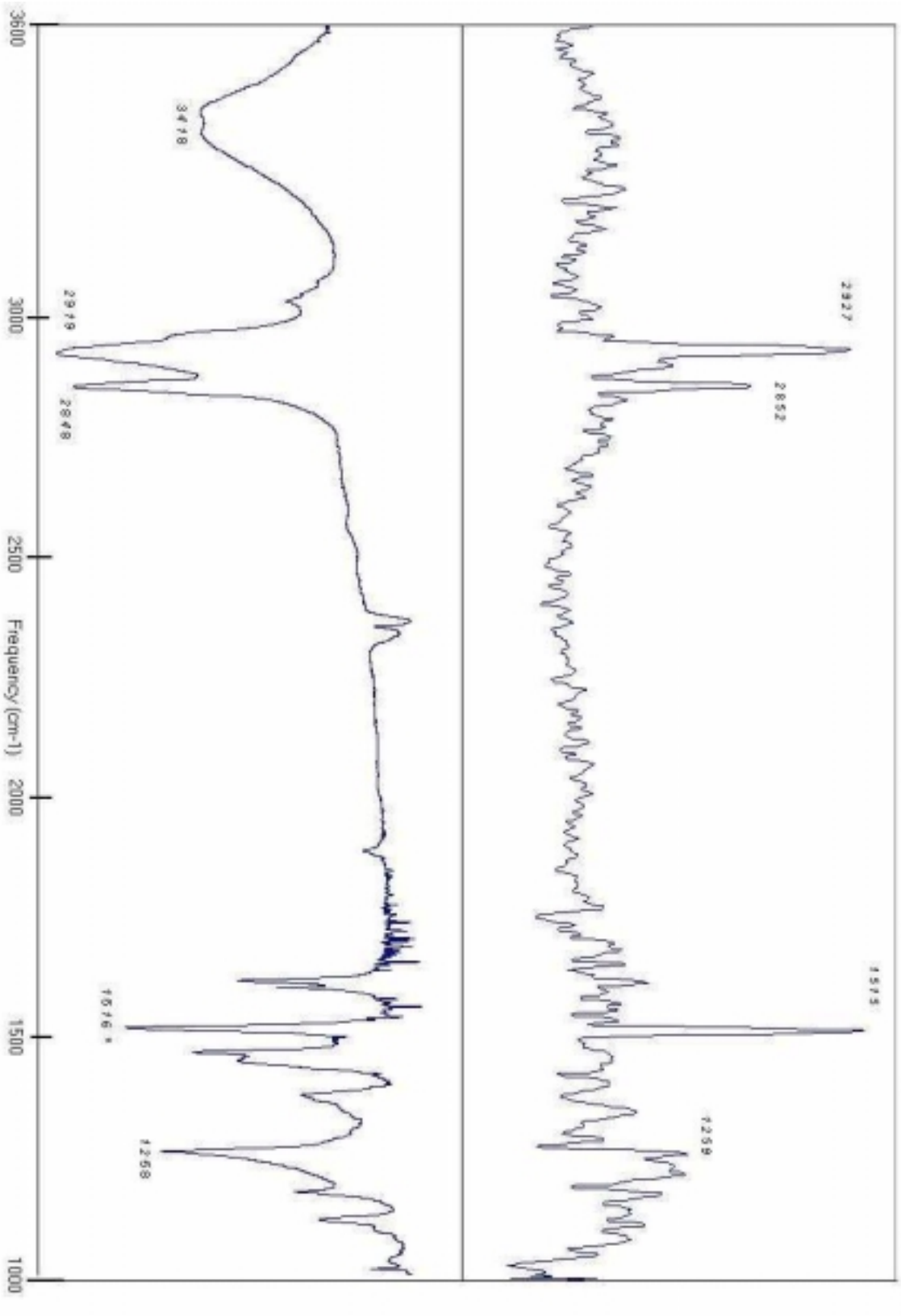

Figure 27 RAIRS and transmission spectrum of 2

3.3.3 Transmission and RAIRS spectra of 16-mercaptohexadecanol (**3**)

The bottom portion of Figure 28 is the Transmission spectrum of thiol **3**. There are only four intense bands that can assigned with confidence. The broad band at 3296 cm^{-1} is due to the terminal –OH stretching mode. Again, DFT calculations overestimate the value of this band by ~ 450 cm^{-1}. The bands at 2927 cm^{-1} and 2855 cm^{-1} are assigned to the symmetric and asymmetric, respectively, C-H stretching modes of the alkyl chain. DFT calculations predict these stretching modes to be 150-160 cm^{-1} higher than the experimentally observed values. The bands at 1462 are assigned to the C-H bending mode of alkyl chain CH_2 groups. The band assignment is consistent with other long chain alkanes.[82] DFT calculations also predict the C-H bend to be at 1480 cm-1 which is in good agreement with the experimentally observed value.

Even though thiol **3** contains a terminal C-O-H group no distinctive C-O stretching frequency is distinctly observed. It is known that C-O stretching modes in alcohols tend to couple to other vibrational modes[82], such as the –OH stretching mode, when closely aggregated (KBr pellet, melt, etc) and tend to appear around 1050 cm^{-1}. There is a broad feature at ~1060 cm^{-1} which is suspected of being due to such coupling but the band assignment is not definitive.

The RAIRS spectrum of SAM **3**, at the top of Figure 28, also shows four distinct bands. The broad feature at ~ 3450 cm^{-1} is believed to be surface adsorbed H_2O. The bands at 2923 cm^{-1} and 2852 cm^{-1} are assigned to the C-H stretching mode of the alkyl chains and correspond well to the C-H stretching frequencies in the transmission spectrum. The band at 1462 cm^{-1} is not very intense but is assigned to the C-H bending of the alkyl chain CH_2 groups.

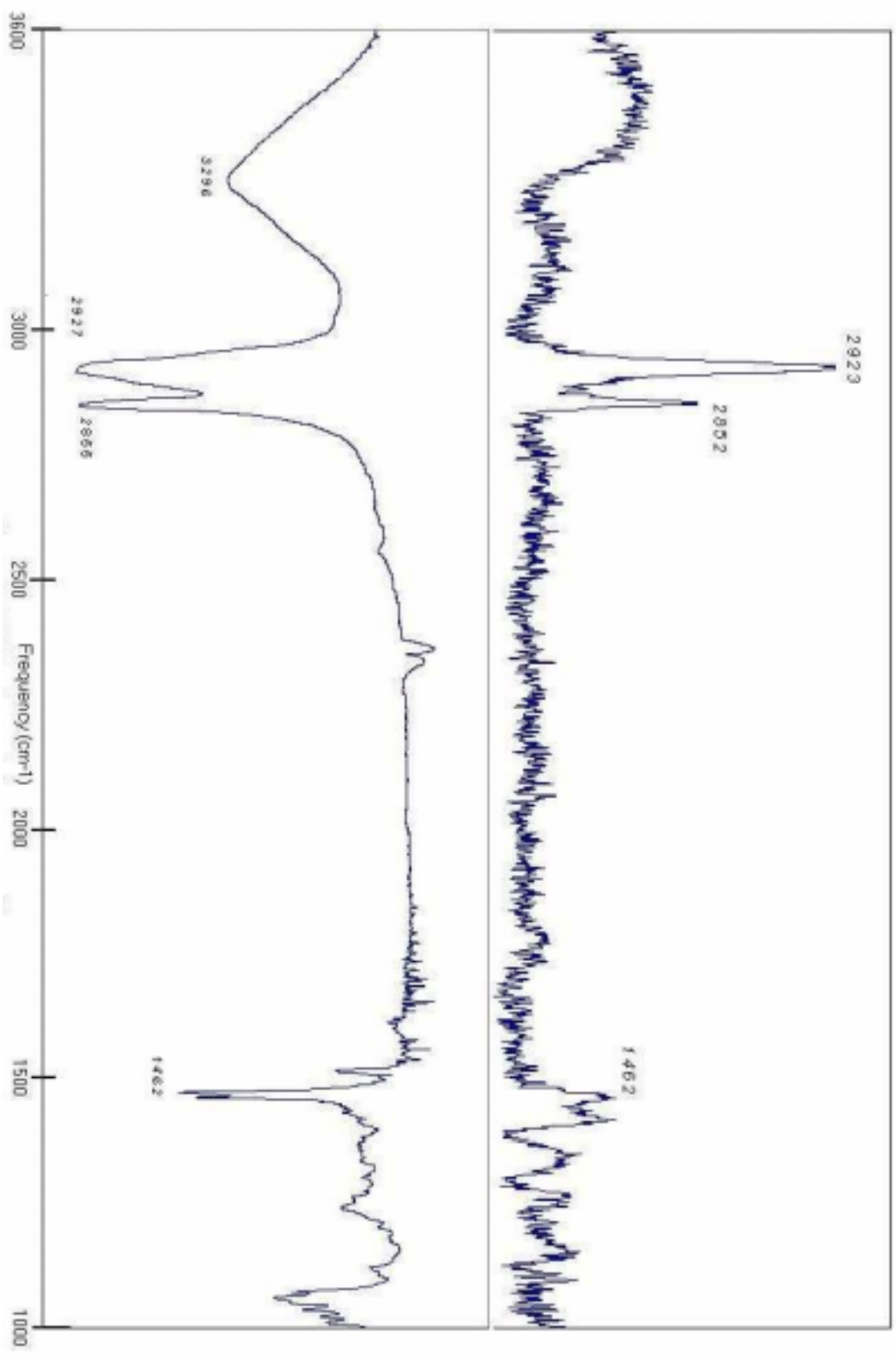

Figure 28 RAIRS and transmission spectrum of 3

3.4 Contact Angle Measurements

In Table 4 are the water contact angle measurements obtained from SAMs of **1**, **2**, and **3**, as well as the contact angles of the silane functionalized SAMs.

Compound	Unfunctionalized	Silane Functionalized
4-(12-mercaptododecyloxy)phenol	$52^{o} \pm 2^{o}$	$78^{o} \pm 2^{o}$
4-(12-mercaptododecyl)phenol	$53^{o} \pm 2^{o}$	$74^{o} \pm 2^{o}$
16-mercaptohexadecanol	$64^{o} \pm 2^{o}$	$75^{o} \pm 2^{o}$
1-decanethiol	$84^{o} \pm 1^{o}$	------

Table 4 Water contact angle measurements for silane functionalized and unfunctionalized SAMs

The contact angle value for SAM **1** indicates a hydrophilic surface, which suggests the terminal –OH groups are not significantly buried in the surface. Upon functionalization with phenyldimethylchlorosilane the contact angle increases 26^{o}. This suggests that the surface hydroxyl groups are accessible for substitution. SAM **2** has similar contact angle values suggesting a similar surface structure. Upon reaction with the silane the contact angle increases 21^{o}. Although the increase in contact angle, upon functionalization for SAM **2**, is not as large as for SAM **1** there is no significant difference in reactivity of hydroxyl groups.

The contact angle value for SAM **3** is 11^{o} higher than SAM **1** and SAM **2** suggesting the surface is less hydrophilic. This suggests the possibility that there is increased surface hydrogen bonding and as a result the O atoms are more buried in the surface. Upon functionalization the contact angle increases 11^{o} to 75^{o} which is nearly identical to the value for fucntionalized SAM **2**. A SAM of decanethiol is included as an example of a hydrophobic surface. Although the contact angles for functionalized SAMs of **1**, **2**, and **3** do not reach the 80^{o} threshold the surfaces can be considered minimally hydrophobic. It is believed that by using a less bulky silanizing

agent more hydroxyl groups can be substituted[84] significantly increasing the water contact angles of the functionalized SAMs.

3.5 RAIRS Spectra of Functionalized and Unfunctionalized SAMS

In the following subsections RAIRS spectra of unfunctionalized and silane functionalized SAMs of **1**, **2**, and **3** are compared and correlated with the contact angle results presented in section 3.4. Section 3.5.1 looks at RAIRS spectra of SAM **1** and SAM **1** functionalized with phenyldimethylchlorosilane. Sections 3.5.2 and 3.5.3 look at RAIRS spectra of SAM **2** and SAM **3** respectively and the effect silanization has on the their surface structure.

3.5.1 RAIRS Spectra of SAM **1** Functionalized and Unfunctionalized

The top spectrum in Figure 29 is the RAIRS spectrum of SAM **1** functionalized with phenyldimethyl-chlorosilane. The band assignments remain the same as are given in section 3.3.1. with the exception of the new band at 1262 cm^{-1}. In section 3.3.1. the broad band at 1241 cm^{-1} is assigned as a C-O stretch but it must be noted that there should be two C-O stretches. Upon functionalization, two bands appear in the C-O stretching frequency region which suggests that prior to functionalization the two bands are overlapping. Contact angles increase 26^{o} and the SAM becomes significantly less hydrophilic. This is easily explained by the addition of hydrophobic silanizing agent to the –OH surface which diminishes the number of surface –OH groups.

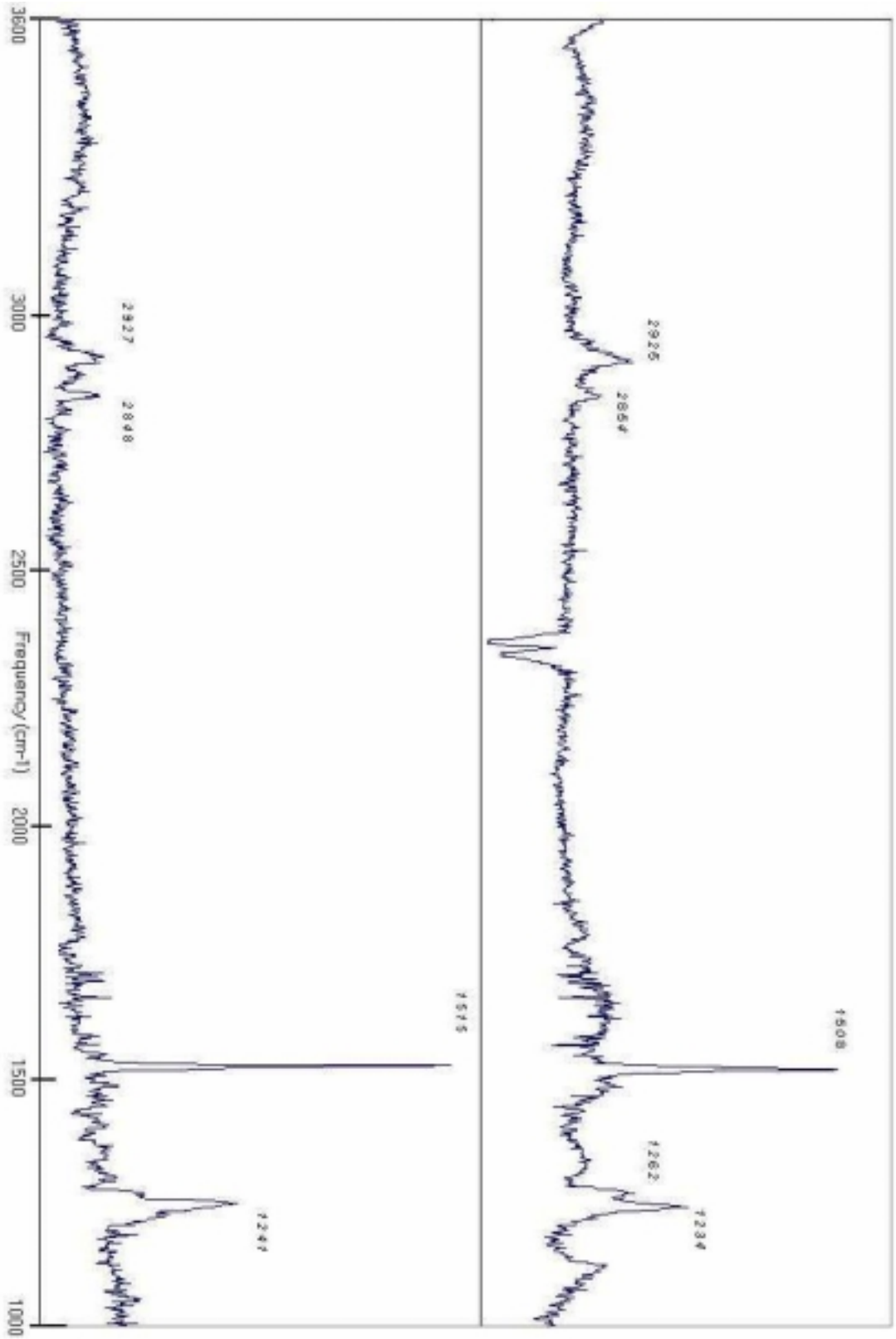

Figure 29 RAIRS spectra of SAM 1 functionalized and unfunctionalized

3.5.2 RAIRS Spectra of SAM **2** Functionalized and Unfunctionalized

The top RAIRS spectrum in Figure 30 is SAM **2** functionalized with phenyldimethychlorosilane. Band assignments remain the same as given in section 3.3.2. The band centered at 1266 cm^{-1} has a larger absorbance value relative to the other bands in the functionalized SAM. This suggests that the C-O stretching mode is more "ether-like". It is known that ether C-O stretching modes are sharper and more intense than phenol or alcohol C-O stretching modes.[82] The new band at 1122 cm^{-1} is tenatively assigned to the Si-O stretching mode of the newly formed Si-O bond. Contact angle measurements suggest the surface is less hydrophilic as a result of silanization and, as with SAM **1**, it is believed that more surface –OH groups can be substituted with the use of a less bulky silanizing agent. Additional silanization may also increase the intensity of the band at 1122 cm^{-1} further corroborating the tentative assignment.

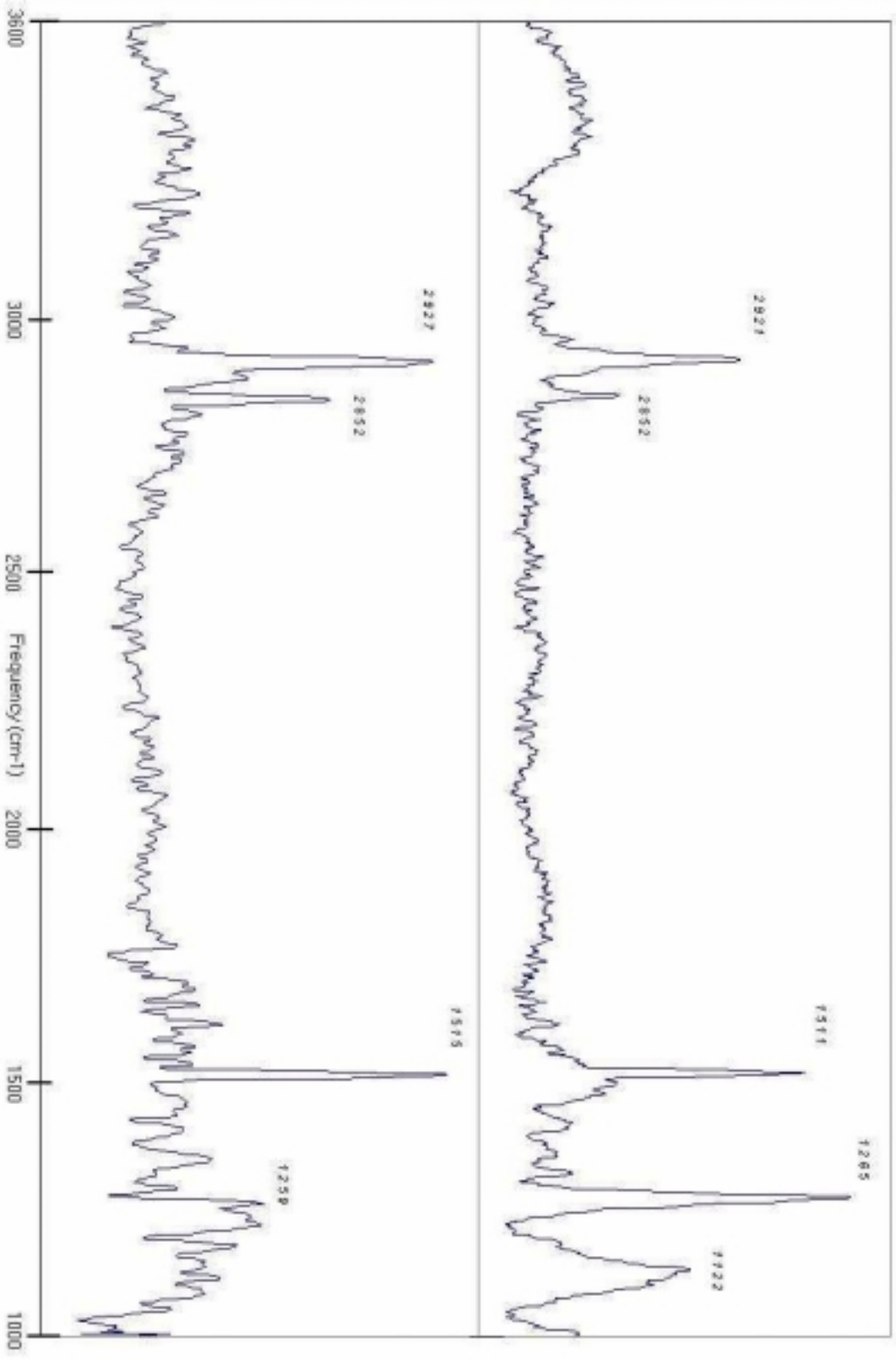

Figure 30 RAIRS spectra of SAM 2 functionalized and unfunctionalized

3.5.3 RAIRS Spectra of SAM 3 Functionalized and Unfunctionalized

The RAIRS spectrum at the top of Figure 31 is SAM **3** functionalized with phenyldimethyl-chlorosilane. Only two band assignments remain the same as those given in section 3.3.3 and correspond to the C-H stretching frequencies. The band at 1268 cm^{-1} is assigned to the C-O stretch of the terminal group. Prior to functionalization the C-O stretch was not distinguishable as is evidenced by the bottom RAIRS spectrum of SAM **3**. Contact angle measurements of functionalized SAM **3** reveal an increase of 11^{o} relative to SAM **3**. The functionalized SAM is only slightly less hydrophilic as a result of functionalization. As discussed in section 3.4, increased surface hydrogen bonding can lend the oxygen atom less susceptible to reaction although the evidence presented is not definitive. It is believed the band at 1462 cm^{-1} from SAM **3** is absent in the top RAIRS spectrum due to silane functionalization. The silane may decrease the packing density of the SAM and reduce the intensity of the C-C stretching mode.

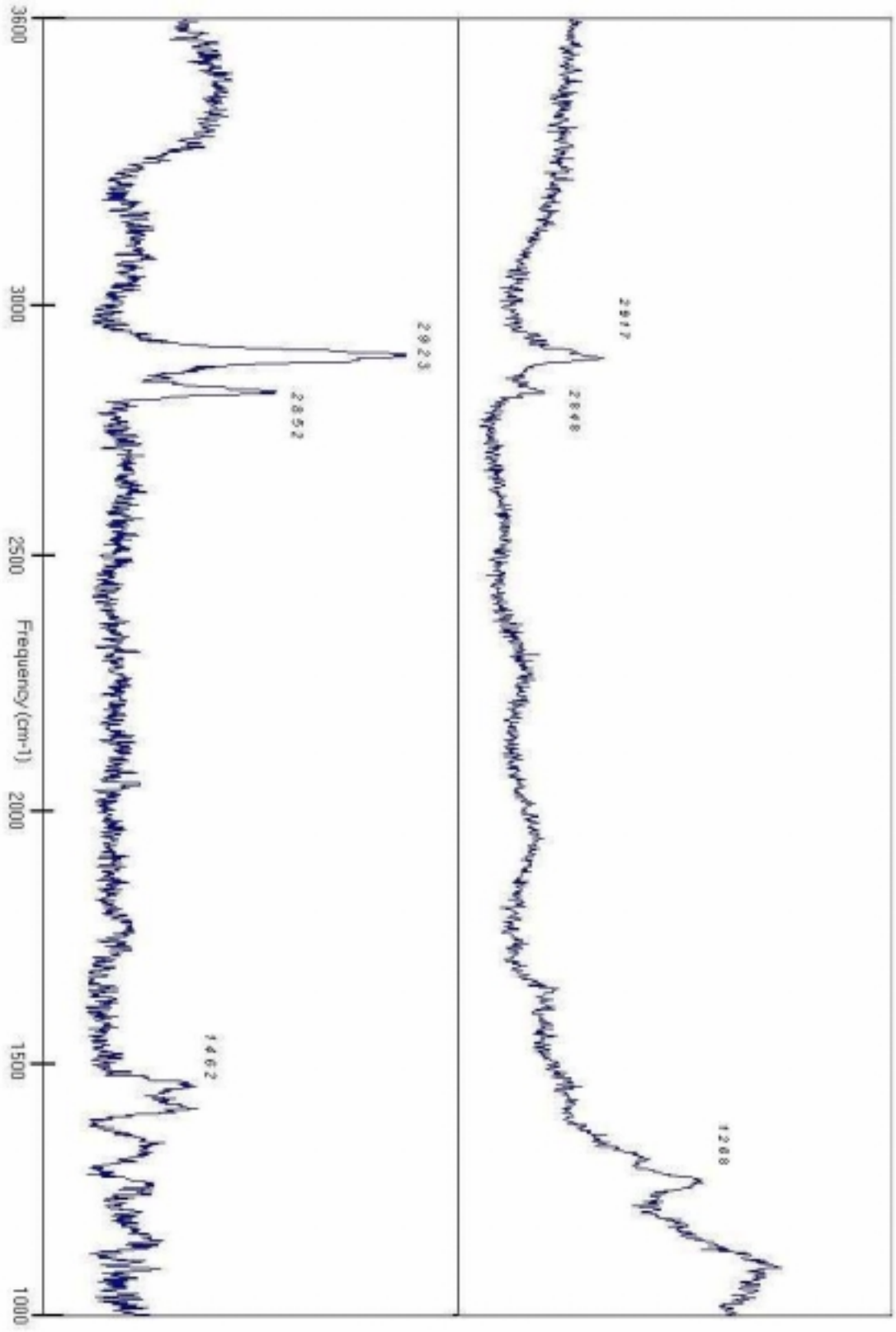

Figure 31 RAIRS spectra of SAM 3 functionalized and unfunctionalized

3.6 Experimental Procedures

In the following subsections experimental procedures are given describing how the DFT calculations are conducted (3.6.1.), how RAIRS spectra were obtained (3.6.2.) and how contact angle measurements were performed (3.6.3.).

3.6.1 DFT Calculations

The DFT calculations were carried out using Titan, a Wavefunction, Inc. software program, installed on a PC. The first step involves drawing the molecule of interest using Titan's graphics program. The energy of the molecule is then minimized using a molecular mechanics minimizer built into Titan. A fixed energy value is obtained after 2-3 minimizations. Following minimization the basis set is picked from several choices given in Titan. The DFT method is then chosen from several available options. Titan provides various outputs, and the vibational modes option must be selected. After these parameters are set the calculation is then started. Calculations for compounds **1**, **2**, and **3** run for approximately 10-12 days. The output file consists of a list of vibrational frequencies. When a particular frequency is selected Titan graphically illustrates the molecular motion giving rise to the vibrational frequency.

3.6.2 RAIRS Spectra

RAIRS spectra were obtained using a Nicolet model 710 infrared spectrometer equipped with a liquid nitrogen cooled HgCdTe detector and interfaced with a PC. Omnic software was used to collect spectra. Spectral resolution was set to 2 cm^{-1} and Boxcar apodization was used and the number of scans set to 512. Spectra were collected at room temperature (25 ^{o}C). Backgrounds were collected daily and substracted from obtained spectra. Spectral files obtained using Omnic software were then converted to (x,y) files using Grams 32 software and imported into Microsoft Excel for plotting.

3.6.3 Contact Angle Measurements

The contact angle measurements were obtained using a Dage 650 model goniometer. Room temperature distilled water was used. A gold slide with a SAM is placed on the sample platform. The goniometer is then focused and the baseline is set to the top of the substrate surface. A 20 μl GC syringe is used to measure a 5 μl drop which is gently placed on the SAM surface. The drop silhouette is focused moving the sample platform horizontally with a mechanical dial. The tangent line dial is used to set a tangent line at the point of contact of the drop with the substrate surface. Contact angles from each side of the drop are measured. The drop is dried using the tip of a Kimwipe and another drop placed on the surface in a different section. A total of five drops are measured for each SAM. The measurements are carried out at room temperature (25^{o}C). Each drop is allowed to equilibrate on the SAM surface for 30 seconds.

3.7 Conclusions

The synthesis of compounds **1**, **2**, and **3** were carried out. SAMs of compounds **1**, **2**, and **3** were formed and analyzed using reflectance IR spectroscopy. The reflectance IR spectra revealed that compounds **1** and **2** would be good models for a silica surface. Functionalization of each SAM surface with phenyldimethylchlorosilane was carried out. Reflectance IR spectra of the functionalized surfaces revealed significant reaction of surface –OH groups with the silane for SAMs of **1** and **2** and to a lesser extent with SAM **3**. Contact angle measurements correlate well with the spectroscopic conclusions. SAMs **1** and **2** are hydrophilic and become minimally hydrophobic upon functionalization. SAM **3** is not as hydrophilic but also becomes minimally hydrophobic upon functionalization. The difference in contact angles between substituted and

unsubstituted SAMs of 16-mercaptohexadecanol is only 11^{o}, which may indicate lower reactivity of surface hydroxyl groups.

The important finding of this thesis is that SAM **1** and **2** are ordered and may serve as good models for silica metallocene immobilization substrates. Contact angles for SAMs **1** and **2** indicate hydrophilic surfaces and fucntionalization studies confirmed the reactivity of their surface hydroxyl groups. SAM surfaces of 16-mercaptohexadecanol are also ordered but surface hydrogen bonding limits the reactivity of surface hydroxides.

3.8 Future Work

The next step in this research is to further characterize SAM **1** and **2** using Surface Enhanced Raman Spectroscopy (SERS). The following step involves reaction of dimethylbromosilyl-substituted zirconocenes with SAM **1** and **2** in the presence of triethylamine as shown below in scheme 8.

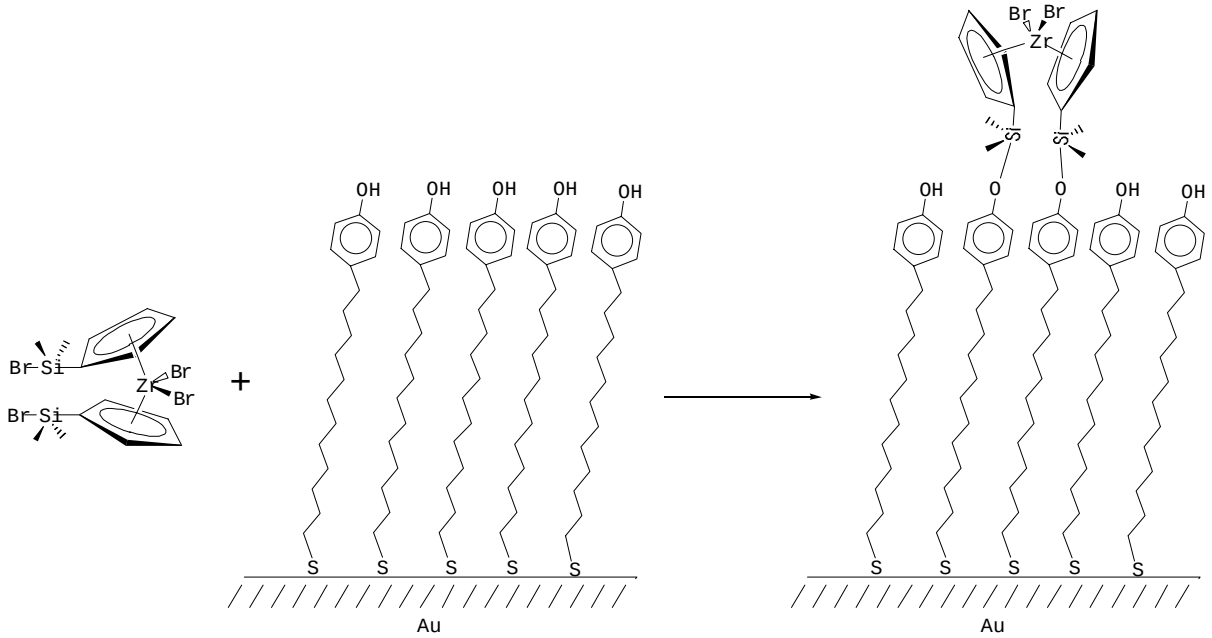

Scheme 8

Zirconocene functionalized SAMs can then be analyzed using RAIRS and SERS, and spectroscopic “fingerprints” for a silica-immobilized single site metallocene catalyst can hopefully be obtained.

Bibliography

(1) Montagna, A. A.; Burkhart, R. M.; Dekmezian, A. H. *Chemtech* 1997, *27*, 26-31.
(2) Sinn, H.; Kaminsky, W. In;; Academic Press,Inc.: New York, 1980; Vol. 18, pp 99-149.
(3) Boor, J. *Ziegler-Natta Catalysts and Polymerizations*; Academic Press: New York, 1979.
(4) Sun, L.; Hsu, C. C.; Bacon, D. W. *J. Polym. Sci. Pol. Chem.* 1994, *32*, 2127-2134.
(5) Bialek, M.; Czaja, K. *Polymer* 2000, *41*, 7899-7904.
(6) Pullukat, T. J.; Hoff, R. E. *Catal. Rev.-Sci. Eng.* 1999, *41*, 389-428.
(7) Forte, M. C.; Coutinho, F. M. B. *Eur. Polym. J.* 1996, *32*, 223-231.
(8) Chien, J. C. W.; Hsieh, J. T. T. *J. Polym. Sci. Pol. Chem.* 1976, *14*, 1915-1932.
(9) Nowlin, T. E.; Klaus, K. P. In *United States Patents*; Mobil Oil Corporation: United States, 1986.
(10) Johnson, B. H. In *United States Patents*; Exxon Research & Engineering Co.: United States, 1984.
(11) Hlatky, G. G. *Chem. Rev.* 2000, *100*, 1347-1376.
(12) Nowlin, T. E.; Mink, R. I.; Lo, F. Y.; Kumar, T. *J. Polym. Sci. Pol. Chem.* 1991, *29*, 1167-1173.
(13) Salajka, Z.; Kratochvila, J.; Hamrik, O.; Kazda, A.; Gheorghiu, M. *J. Polym. Sci. Pol. Chem.* 1990, *28*, 1651-1660.
(14) Nowlin, T. E.; Kissin, Y. V.; Wagner, K. P. *J. Polym. Sci. Pol. Chem.* 1988, *26*, 755-764.
(15) Nowlin, T. E.; Klaus, K. P. In *United States Patents*; Mobil Oil Corporation: United States, 1984.
(16) Nowlin, T. E. In *United States Patents*; Mobil Oil Corporation: United States, 1986.
(17) Eley, D. D.; Keir, D. A.; Rudham, R.
(18) Soga, K. *Polymer* 1973, *5*, 128.
(19) Kissin, Y. V. *Isospecific Polymerization of Olefins*; Springer-Verlag: New York, 1985.
(20) Gianui, U.; Mayr, A.; Longi, P.; Susa, E.; Davoli, V.; Deluca, D.; Leccese, A.; Pricca, A. In *Ger. Offen*; Montecattini Elison S.P.A: Germany, 1971.
(21) Kashiwa, N. In;; Mitsui Petrochemical Industries: Japan, 1975.
(22) Wilkinson, G.; Pauson, P. L.; Birmingham, J. M.; Cotton, F. A. *J. Am. Chem. Soc.* 1953, *75*, 1011-1012.
(23) Breslow, D. S.; Newburg, N. R. *J. Am. Chem. Soc.* 1957, *79*, 5072.
(24) Natta, G.; Pino, P.; Mazzanti, G.; Giannini, U. *J. Am. Chem. Soc.* 1957, *79*, 2975-2976.
(25) Andresen, A.; Cordes, H.-G.; Herwig, J.; Kaminsky, W.; Merck, A.; Mattwe, R.; Pein, J.; Sinn, H.; Vollmer, H.-G. *Angew. Chem. Inter. Ed. Engl.* 1976, *15*, 630-632.
(26) Sinn, H.; Kaminsky, W.; Vollmer, H.-J.; Woldt, R. *Angew. Chem. Int. Ed. Engl.* 1980, *19*, 390-392.
(27) Kaminaka, M.; Soga, K. *Polymer* 1992, *33*, 1105-1107.
(28) Satyanarayana, G.; Sivaram, S. *Macromolecules* 1993, *26*, 4712-4714.
(29) SenSarma, S.; Sivaram, S. *Macromol. Chem. Phys.* 1997, *198*, 495-503.
(30) Brockmeier, N. F. In;; Quirk, R. P., Ed.; Cambridge University Press: New York, 1983; pp 671-696.
(31) Bailly, J.-C.; Bres, P.; Chabrand, C.; Daire, E. In *United States Patents*; BP Chemicals Limited: United States, 1992.
(32) Soga, K.; Arai, T.; Uozumi, T. *Polymer* 1997, *38*, 4993-4995.
(33) Sensarma, S.; Sivaram, S. *Macromol. Chem. Phys.* 1999, *200*, 323-329.
(34) Marks, T. J. *Accounts Chem. Res.* 1992, *25*, 57-65.
(35) Buys, I. E.; Hambley, T. W.; Houlton, D. J.; Maschmeyer, T.; Masters, A. F.; Smith, A. K. *Journal of Molecular Catalysis* 1994, *86*, 309-318.
(36) Duchateau, R.; Abbenhuis, H. C. L.; van Santen, R. A.; Thiele, S. K. H.; van Tol, M. F. H. *Organometallics* 1998, *17*, 5222-5224.
(37) Hong, S. C.; Ban, H. T.; Kishi, N.; Jin, J. Z.; Uozumi, T.; Soga, K. *Macromol. Chem. Phys.* 1998, *199*, 1393-1397.
(38) Alt, H. G. *J. Chem. Soc.-Dalton Trans.* 1999, 1703-1709.
(39) Arai, T.; Ban, H. T.; Uozumi, T.; Soga, K. *Macromol. Chem. Phys.* 1997, *198*, 229-237.
(40) Lee, D. H.; Yoon, K. B.; Noh, S. K. *Macromol. Rapid Commun.* 1997, *18*, 427-431.
(41) Noh, S. K.; Kim, S.; Kim, J.; Lee, D. H.; Yoon, K. B. *J. Polym. Sci. Pol. Chem.* 1997, *35*, 3717-3728.
(42) Iler, R. K. *The Chemistry of Silica: Solubility, Polymerization, Colloid and Surface Properties, and Biochemistry*; Wiley: New York, 1979.
(43) Peri, J. B.; Jr., A. L. H. *The Journal Of Physical Chemistry* 1968, *72*, 2926-2933.

(44) dos Santos, J. H. Z.; Krug, C.; da Rosa, M. B.; Stedile, F. C.; Dupont, J.; Forte, M. D. *J. Mol. Catal. A-Chem.* 1999, *139*, 199-207.
(45) dosSantos, J. H. Z.; Dorneles, S.; Stedile, F. C.; Dupont, J.; Forte, M. M. D.; Baumvol, I. J. R. *Macromol. Chem. Phys.* 1997, *198*, 3529-3537.
(46) dos Santos, J. H. Z.; Greco, P. P.; Stedile, F. C.; Dupont, J. *J. Mol. Catal. A-Chem.* 2000, *154*, 103-113.
(47) Collins, S.; Kelly, W. M.; Holden, D. A. *Macromolecules* 1992, *25*, 1780-1785.
(48) Welborn, J., H.C In *United States Patents*; Exxon Chemical Patents Inc: United States, 1989.
(49) Takahashi, T. In *United States Patents*; Mitsubishi Petrochemical Co. Ltd.: United States, 1991.
(50) Ernst, E.; Reussener, J. N. In *J. Eur. Pat. Appl*, 1997.
(51) Kuber, F.; Bachmann, B.; Spaleck, W.; Winters, A. In *United States Patents*; Targor Gmbh: United States, 1998.
(52) Kuber, F.; Bachmann, B.; Spaleck, W.; Winter, A. In *United States Patents*; Targor Gmbh: Unietd States, 2000.
(53) Fritze, C.; Kuber, F.; Bohnen, H. In *United States Patents*; Targor Gmbh: United States, 2000.
(54) Becker, R.-F.; Rieger, R. In *United States Patents*; Witco Gmbh: United States, 2000.
(55) Fraaije, V.; Bachmann, B.; Winter, A. In *Eur. Pat. Appl.*, 1997.
(56) Brinen, J. L.; Speca, A. N.; Tormaschy, K.; Russell, K. A. In *United States Patents*; Exxon Chemical Patents Inc.: United States, 1997.
(57) Brinen, J. L.; Speca, A. N.; Tormarschy, K.; Russell, K. A. In *United States Patents*; Exxon Chemical Patents Inc.: United States, 1997.
(58) Brinen, J. L.; Speca, A. N.; Tormarschy, K.; Russell, K. A. In *United States Patents*; Hoechst: United States, 1998.
(59) Nowlin, T. E.; Lo, F. Y.; Shinomoto, R. S.; Shirodkar, P. P. In *United Sates Patents*; Mobil Oil Corporation: United States, 1994.
(60) Lee, B. Y.; Oh, J. S. *J. Organomet. Chem.* 1998, *552*, 313-317.
(61) Langhauser, F.; Fischer, D.; Kerth, J.; Schweier, G.; Barsties, E.; Brintzinger, H.-H.; Schaible, S.; Roell, W. In *United States Patents*; Bask Aktlengesellschaft: United States, 1997.
(62) Suzuki, N.; Asami, H.; Nakamura, T.; Huhn, T.; Fukuoka, A.; Ichikawa, M.; Saburi, M.; Wakatsuki, Y. *Chem. Lett.* 1999, 341-342.
(63) Iiskola, E. I.; Timonen, S.; Pakkanen, T. T.; Harkki, O.; Lehmus, P.; Seppala, J. V. *Macromolecules* 1997, *30*, 2853-2859.
(64) Lindblad, T.; Rebenstorf, B. *J. Chem. Soc.-Faraday Trans.* 1991, *87*, 2473-2478.
(65) Juvaste, H.; Pakkanen, T. T.; Iiskola, E. I. *Organometallics* 2000, *19*, 1729-1733.
(66) Slotfeldt-Ellingsen, D.; Dahl, I. M.; Ellestad, O. H. *Journal of Molecular Catalysis* 1980, *9*, 423-434.
(67) Xu, J. T.; Zhao, J.; Fan, Z. Q.; Feng, L. X. *Macromol. Rapid Commun.* 1997, *18*, 875-882.
(68) Deck, P. A.; Fischer, T. S.; Downey, J. S. *Organometallics* 1997, *16*, 1193-1196.
(69) Ulman, A. *Chem. Rev.* 1996, *96*, 1533-1554.
(70) Ulman, A. *An Introduction to Ultrathin Organic Films: from Langmuir-Blodgett to Self-assembly*; Academic Press: San Diego, 1991.
(71) Ulman, A. *Characterization of Organic Thin Films: Materials Characterization Series-Surfaces, Interfaces, Thin Films*; Butterworth-Heinemann: Stoneham, MA, 1995.
(72) Dubois, L. H.; Nuzzo, R. G. *Annual Review of Physical Chemistry* 1992, *43*, 437-463.
(73) Bishop, A. R.; Nuzzo, R. G. *Current Opinions Colloid and Interface Science* 1996, *1*, 127-136.
(74) Taylor, C. D. In *Chemistry*; Virginia Tech: Blacksburg, 2000; p 85.
(75) Greenler, R. G. *Journal of Chemical Physics* 1965, *44*, 310-315.
(76) Pangborn, A. B.; Giardello, M. A.; Grubbs, R. H.; Rosen, R. K.; Timmers, F. J. *Organometallics* 1996, *15*, 1518-1520.
(77) Pemble, M. E. In *Surface Analysis: The principal techniques*; Vickerman, J. C., Ed.; John Wiley & Sons: West Sussex, 1997.
(78) Hu, C.-H.; Chong, D. P. In *Encyclopedia of Computational Chemistry*, 1998; Vol. 1, pp 664-678.
(79) Johnson, B. G.; Gill, P. M. W.; Pople, J. A. *Journal of Chemical Physics* 1993, *98*, 5612-5626.
(80) In;; Wavefunction, Inc.: Irvine, 1999.
(81) Kwok, D. Y.; Neuman, A. W. In *Surface Characterization Methods: Principles, Techniques, and Applications*; Milling, A. J., Ed.; Marcel Dekker,Inc.: Durham, 1999; Vol. 87.
(82) Silverstein, R. M.; Bassler, C. G.; Morrill, T. C. *Spectrometric Identification of Organic Compounds*; 5th ed.; John Wiley & Sons, Inc.: New York, 1991.

(83) Whitesides, G. M.; Laibinis, P. E.; Allara, D. L.; Tao, Y.-T.; Parikh, A. N.; Nuzzo, R. G. *J. Am. Chem. Soc.* 1991, *113*, 7152-7167.
(84) McCarthy, T. J.; Fadeev, A. Y. *Langmuir* 1999, *15*, 3759-3766.

Vita

The author was born on April 3, 1971 in Pontevedra, Spain. He attended the Minor Seminary in Santiago de Compostela and A.C. Reynolds High School graduating in June of 1989. He attended the University of North Carolina at Asheville and received a Bachelor of Science degree in May of 1994. He worked for Roche Biomedical in Research Triangle Park inDurham, North Carolina for 3 years. Following his stance at Roche he sought admission to Virginia Tech's graduate chemistry program to obtain his Ph.D.